

# Chirogenesis in Zinc Porphyrins: Theoretical Evaluation of Electronic Transitions, Controlling Structural Factors and Axial Ligation

Irina Osadchuk,<sup>\*[a, b]</sup> Riina Aav,<sup>[a]</sup> Victor Borovkov,<sup>[a]</sup> and Eric Clot<sup>[b]</sup>

In the present work, sixteen different zinc porphyrins (possessing different *meso* substituents) with and without a chiral guest were modelled using DFT and TD-DFT approaches in order to understand the influence of various controlling factors on electronic circular dichroism (ECD) spectra. Two major aspects are influenced by these factors: excitation energy of the electronic transitions and their intensity. In the case of excitation energy, the influence increases in the following order:

orientation of the peripheral substituents < substituent's nature < axial ligation. However, the deformation of the porphyrin plane does not affect the excitation energies. In the case of intensity, the influence increases as follows: substituent's nature < conrotatory orientation of the peripheral substituents < deformation of the porphyrin plane < disrotatory orientation of the peripheral substituents < axial ligation.

## 1. Introduction

Porphyrins and their derivatives are involved in a diversity of biological processes, such as cell respiration, oxygen transport, light harvesting and fatty acid oxidation.<sup>[1–3]</sup> Synthetic porphyrins also found a broad application in catalysis,<sup>[4–6]</sup> optical and chemo sensors,<sup>[7–15]</sup> light harvesting,<sup>[5,16–18]</sup> medicine,<sup>[19–22]</sup> supramolecular systems,<sup>[1,23–27]</sup> electronic devices,<sup>[11,28,29]</sup> etc. Specific natural and supramolecular chiral environment may result in chirogenic processes in porphyrin chromophores, which can be detected by various spectroscopic methods such as X-ray,<sup>[30–33]</sup> IR,<sup>[31,34]</sup> Raman,<sup>[32]</sup> NMR,<sup>[31,32,35,36]</sup> circular polarized luminescence,<sup>[30,37,38]</sup> vibrational,<sup>[34,39,40]</sup> electronic (ECD),<sup>[9,19,41–44]</sup> and magnetic<sup>[34,45,46]</sup> circular dichroism.


However, the question of ECD induction mechanisms in mono-porphyrins and their derivatives from the theoretical point of view is still not fully resolved. Initially, the low energy shift in absorption (and correspondingly ECD) spectra was explained by the substituents inducing a nonplanar deformation,<sup>[32,47–52]</sup> but in 2000 Wertsching et al.<sup>[53]</sup> reported


that the electronic effects of substituent and in plane nuclear reorganization have the main impact on this phenomenon. Ryeng and Ghosh<sup>[54]</sup> also agreed that the in plane nuclear reorganization is able to shift the absorption bands to low energy, however, they stated that structural ruffling brings a significant perturbation in the electronic structure of porphyrin and hence causes a red shift of both the B- and Q-bands. In 2003, Haddad et al.<sup>[55]</sup> showed a strong correlation between ruffling of the porphyrin plane and red-shift in the absorption energy and suggested to use this shift as a diagnostic tool of the non-planarity upon exclusion of the influence of electronic and structural factors brought by substituents. This is in agreement with the works of Song et al.<sup>[52]</sup> and Zhou et al.,<sup>[56,57]</sup> which reported that the electronic spectra showed a gradual red shift upon increasing the degree of distortion. However, Cramariuc et al.<sup>[51]</sup> stated that the distortions of the porphyrin ring contribute only about 20% to the red shifts of the absorption peaks. This is in agreement with the conclusion of Guberman-Pfeffer et al.<sup>[58]</sup> and Thomassen et al.<sup>[59]</sup> that non-planarity accounts only in part for the observed shift. In 2016, Graves et al.<sup>[60]</sup> reported a nonlinear dependence of the B-band shifts. Thus, in iron porphyrins blue shifts of the B-bands correspond to small distortions of up to 1.0 Å and red shifts to distortions of up to 2.3 Å.

In many works, the influence of a perturbation of the porphyrin electronic structure on the energy of frontier orbitals and the corresponding absorption spectra, both experimentally<sup>[59,61–64]</sup> and theoretically,<sup>[59,61,63,65,66]</sup> was investigated. Different substituents at both the  $\beta$ -<sup>[59,61,63,65–67]</sup> and *meso*-<sup>[61,62,65,68,69]</sup> positions of the porphyrin ring were studied and it was shown that the substituents changed the energy of frontier orbitals<sup>[51,62,65,66,68,69]</sup> and lowered the symmetry of the molecule,<sup>[51,70]</sup> which resulted in broadening<sup>[61,63,70]</sup> and red<sup>[51,61,65,67,70]</sup> or blue<sup>[63,71]</sup> shifting of the B- and Q-absorption bands. Also, peripheral substituents can significantly change the nature of the frontier orbitals by localizing electron density

[a] Dr. I. Osadchuk, Prof. Dr. R. Aav, Prof. Dr. V. Borovkov  
Department of Chemistry and Biotechnology  
School of Science  
Tallinn University of Technology  
Address Akadeemia tee 15  
12618 Tallinn (Estonia)  
E-mail: irina.osadchuk@taltech.ee

[b] Dr. I. Osadchuk, Dr. E. Clot  
ICGM, Univ Montpellier  
CNRS, ENSCM Montpellier (France)

 Supporting information for this article is available on the WWW under <https://doi.org/10.1002/cphc.202100345>

 © 2021 The Authors. ChemPhysChem published by Wiley-VCH GmbH. This is an open access article under the terms of the Creative Commons Attribution Non-Commercial NoDerivs License, which permits use and distribution in any medium, provided the original work is properly cited, the use is non-commercial and no modifications or adaptations are made.

on the substituents instead of the  $\pi$ -system of the porphyrin ring.<sup>[61–63]</sup> LeCours et al.<sup>[62]</sup> showed based on the absorption spectra of [5,15-bis(aryl)ethynyl]-10,20-diphenylporphyrinato]zinc (II) complexes, that the energies of the B- and Q-bands are blue shifted as the aryl substituents at the *meso*-position become less electron donating. In 2008, Hayashi et al.<sup>[70]</sup> reported that expansion of the  $\pi$ -system in the fused-Zn porphyrins broadens and shifts the B- and Q-bands to lower energy. A year later, Lee et al.<sup>[61]</sup> showed that the  $\pi$ -conjugation in both the *meso*- and  $\beta$ -substituents of Zn porphyrins causes broadening and red shifting of the absorption bands as well as corresponding intensity enhancement with increased  $\pi$ -conjugation. In 2010, Göransson et al.<sup>[72]</sup> suggested that the red shift in absorption is more affected by the substituent's extended  $\pi$ -conjugation, while the broadening of the B-band is more influenced by the substituent's position. Ma et al.<sup>[73]</sup> showed that the HOMO-LUMO gap increases along with the change of the substituent's properties from electron-withdrawing to electron-donating. In 2012 Barbee et al.<sup>[74]</sup> concluded that the HOMO-LUMO energy gap increases for both the *meso*- and  $\beta$ -substituents in nickel porphyrins in the following order:  $\text{CH}_3 > \text{Br} > \text{CF}_3 > \text{NO}_2$ . Also, in 2018 Hajizadeh et al.<sup>[75]</sup> showed that replacement of the  $\pi$ -electron bridge substituents at the *meso*-positions of zinc porphyrin can increase the LUMO energy level. Additionally, it was found that perturbation of the electronic structure may be achieved by incorporation of a hetero atom into the porphyrin core.<sup>[58,76–78]</sup>

Beside internal chemical modification of the porphyrin chromophore, external interactions, such as axial ligation, may play a significant role in the ECD behavior, since it affects the charge<sup>[79]</sup> and the spin state<sup>[52,80]</sup> of the central metal ion, the electronic configuration,<sup>[52,60,81–84]</sup> and the planarity of the porphyrin molecule.<sup>[44,57,79,85–90]</sup> Kolling et al.,<sup>[91]</sup> Wang et al.,<sup>[79]</sup> and Song et al.<sup>[52]</sup> showed that the axial ligation induced a red shift of the B-bands, whilst a blue shift<sup>[92]</sup> was also observed depending on a metal ion. Wang et al.<sup>[93]</sup> and Walters et al.<sup>[69]</sup> reported that the axial ligation selectively increases the  $a_{2u}$  orbital energy in various zinc porphyrins.

Moreover, it is known that ECD spectra are sensitive to variations in the environment and depend upon electronic coupling with the porphyrin's peripheral substituents as it was shown by Blauer et al.,<sup>[94]</sup> Kobayashi et al.,<sup>[95]</sup> and Nagai et al.<sup>[96]</sup> For example, in 1993 Blauer et al.<sup>[94]</sup> reported that the electronic transitions in the B absorption region are a result of coupling between the prosthetic heme  $\pi$ - $\pi^*$  electric dipole moments and dipole moments of the proximate aromatic amino acid residues. Also, Kobayashi et al.<sup>[95]</sup> explained how the chiral peripheral binaphthyl groups are able to induce ECD in achiral phthalocyanines and determine the sign of ECD spectra. Further, Nagai et al.<sup>[96]</sup> showed that replacement of the 2,4-vinyl side chains in the heme prosthetic group of myoglobin decreased the intensity of B-band, while change of the 6,7-diacetate substituents with carboxylates resulted in disappearance of the positive ECD band in the B absorption region. Angelini et al.<sup>[97]</sup> explained the split ECD signal as electronic communication between two chromophores.

In our previous works<sup>[98,99]</sup> we showed that the conformation of a chiral guest determines the shape of the induced ECD spectra of achiral porphyrins upon axial ligation. In the present work we discuss the electronic and geometry factors and their respective contribution, which may affect the porphyrin electronic transitions and subsequently the corresponding ECD spectra. In particular, four different factors have been analyzed. First, the influence of pure electronic effects was considered. For this purpose, zinc porphyrins with a flat macrocyclic structure, which electronic properties are tuned by varying the peripheral *meso*-substituents, were modelled. Second, the influence of the spatial orientation (tilt) of the peripheral *meso*-substituents on the electronic transitions was investigated. In this part, the porphyrin planes were specifically kept planar, whilst the dihedral angle of the peripheral substituent's tilt was changed. In the third part, the effect of porphyrin distortion was discussed. In this case, the investigated porphyrins were symmetrically distorted, while the corresponding peripheral substituents were fixed perpendicular to the porphyrin plane and coplanar to each other. Finally, the role of the axial ligation was investigated.

## 2. Results and Discussion

### 2.1. Model Systems

In this study sixteen zinc porphyrins, which differed by two peripheral *meso*-substituents at the  $C_{meso}$  positions, were chosen as corresponding model systems and hosts for external ligation (Figure 1). The choice of zinc complexes was dictated by their preference to adopt a penta-coordinated geometry with axial coordination of various functional guests not altering the planarity of the porphyrin ring.<sup>[71]</sup>

In the present work, the *meso*-position was chosen for peripheral substitutions, since it does not significantly distort the porphyrin plane,<sup>[100,101]</sup> that is an important aspect for our study, in contrast to the  $\beta$ -substituents.<sup>[67,102–106]</sup> Essentially, two substituents at the 5- and 15-positions were chosen and classified to be either neutral (R=H, Ph), with electron-donating ( $\text{CH}_3$ ,  $\text{NMe}_2$ ,  $\text{OMe}$ ,  $\text{Ph-Me-}p$ ,  $\text{Ph-NMe}_2-p$ ,  $\text{Ph-OMe-}p$ ,  $\text{C}\equiv\text{C-Ph-NMe}_2-p$ ), or electron-withdrawing ( $\text{CF}_3$ ,  $\text{NO}_2$ ,  $\text{CN}$ ,  $\text{F}$ ,  $\text{OC(O)H}$ ,  $\text{Ph-CF}_3-p$ ,  $\text{C}\equiv\text{C-Ph-NO}_2-p$ ) groups. Besides, some substituents can serve as secondary chromophores (in the case of  $\text{OC(O)H}$ ,  $\text{NO}_2$ ,  $\text{Ph}$  and its derivatives). It is of note that several functionalized Ph substituents were analyzed. Though these substituents usually do not have electron density in their frontier molecular orbitals resulting in a minor influence on the electronic structure,<sup>[59,69,71,101,103,107]</sup> they serve as secondary chromophores, the properties of which can easily be tuned by changing the functional groups at the Ph ring. Also, it should be noted that the *meso*-substituents cover only a part of the electronic perturbations. The HOMO ( $a_{2u}$ ) is heavily populated at the *meso*-carbons and has reduced density at the  $\beta$ -carbons in contrast to the  $a_{1u}$  orbital, where the electron density is localized at both the  $\alpha$ - and  $\beta$ -carbons (Figure 2).<sup>[68,69]</sup> As a chiral guest, (*R*)-2-aminobutane was chosen as one of the simplest

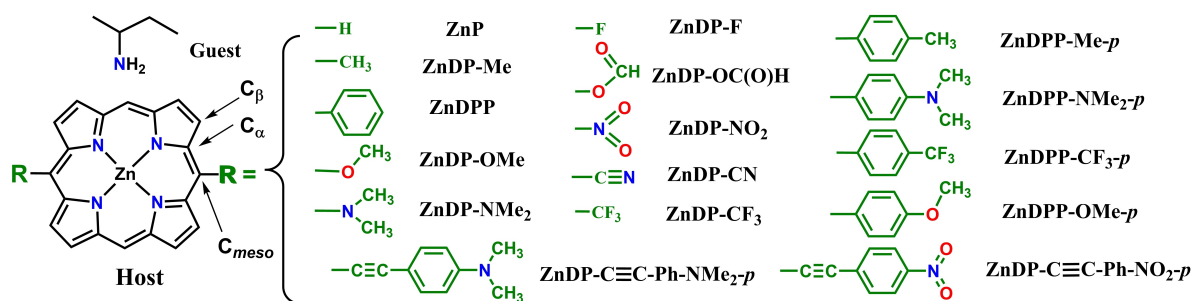


**Figure 1.** Structures of guest (*(R)*-2-aminobutane) and porphyrin hosts with various substituents (ZnP, ZnDP-Me, ZnDPP, ZnDP-OMe, ZnDP-NMe<sub>2</sub>, ZnDP-F, ZnDP-OC(O)H, ZnDP-NO<sub>2</sub>, ZnDP-CN, ZnDP-CF<sub>3</sub>, ZnDPP-Me-*p*, ZnDPP-NMe<sub>2</sub>-*p*, ZnDPP-CF<sub>3</sub>-*p*, ZnDPP-OMe-*p*, ZnDP-C≡C-Ph-NMe<sub>2</sub>-*p*, ZnDP-C≡C-Ph-NO<sub>2</sub>-*p*) used as model systems for ECD spectral simulations.

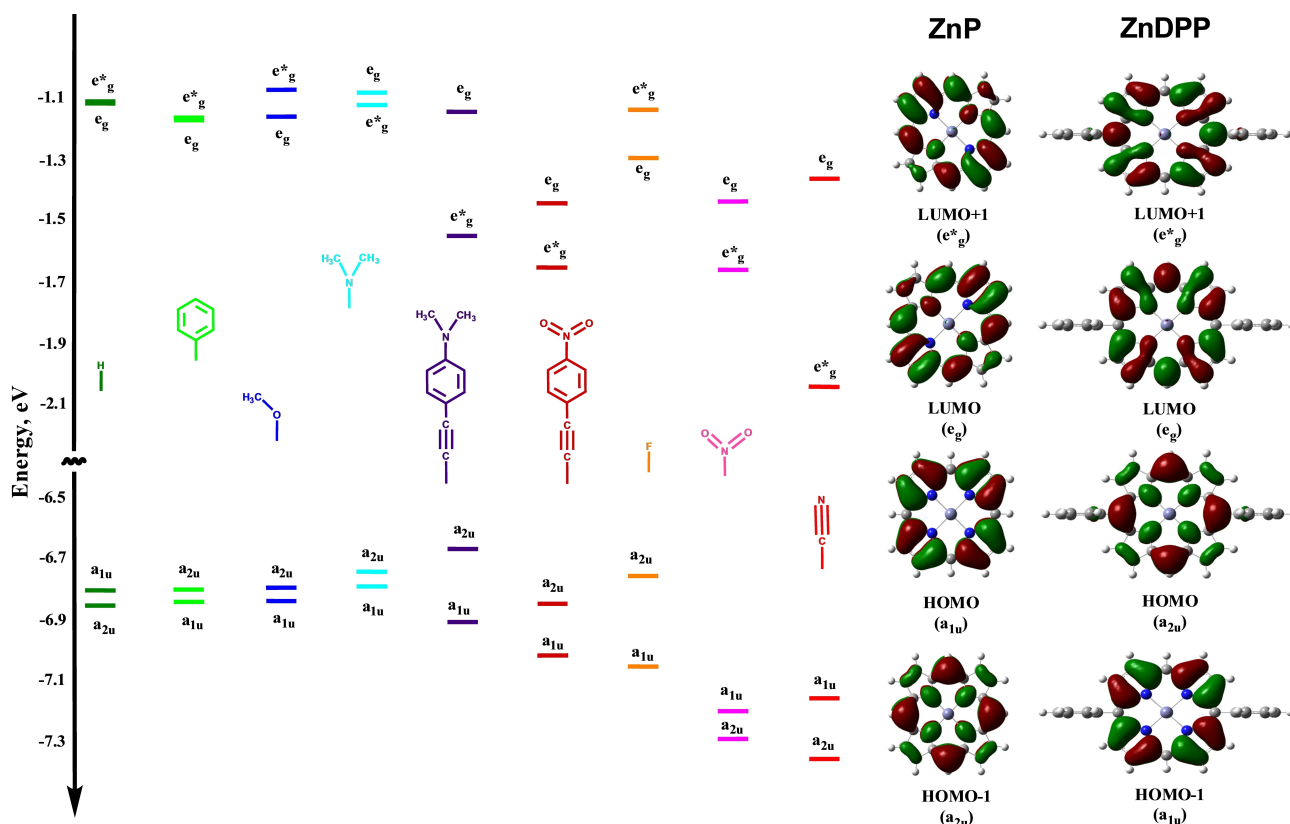


**Figure 2.** Energies of the frontier orbitals involved into the electronic transitions of several flat zinc porphyrins with various orthogonal substituents calculated using  $\omega$ B97X-D/cc-pVTZ and visualisation of frontiers orbitals for ZnP and ZnDPP.

enantiopure molecule. Furthermore, (*R*)-2-aminobutane does not contain any chromophoric group and thus, its positional and conformational changes have minor influence on ECD spectra.<sup>[108]</sup> Dichloromethane was chosen as one of the most commonly used solvents for ECD spectroscopy of porphyrins.

Although a racemic mixture and/or free rotation of the peripheral substituents and guest molecules are present in a real solution, and the corresponding association constant and concentration play an important role in the intensities and shape of ECD spectra, these dynamic factors were not considered in this work. In all of the molecules shown below, a part of or the whole molecular skeleton was fixed in a certain

position and the corresponding calculations were carried out in order to understand how the particular factor affects the electronic transitions and subsequently the ECD spectrum.

## 2.2. Influence of the Electronic Effects

The absorption and ECD spectra of porphyrins and their host-guest complexes typically have two absorption regions: 500–650 and 350–450 nm corresponding to the Q- and B-bands with two electronic transitions in each band.<sup>[109,110]</sup> As a result of the forbidden character,<sup>[45]</sup> intensities of the Q-bands are small and

therefore in the present work only the B-bands will be considered.

It is well known that the electronic structure of a porphyrin can be changed by adding peripheral substituents with either electron-donating or electron-withdrawing effects,<sup>[74,75,111–114]</sup> which cause the  $\pi$ -electron density to redistribute over the macrocycle.<sup>[115,116]</sup> However, addition of peripheral substituents usually generates some distortion of the porphyrin plane,<sup>[74,75,111–113]</sup> hence increasing steric and/or electrostatic repulsion between the substituents.<sup>[41]</sup> In general, ECD spectra are sensitive to both the electronic and conformational factors,<sup>[74,94,113,117]</sup> therefore in order to exclude any conformational contribution, the six first electronic transitions in structurally flat zinc porphyrins were calculated. Corresponding geometries were obtained by optimization with frozen dihedral angles of all non-hydrogen atoms in the porphyrin plane, while the peripheral substituents were fixed in the orthogonal ( $90^\circ$ ) position to the flat porphyrin plane (Figure 2). This procedure was designed to avoid additional coupling of the porphyrin's and substituent's dipole moments,<sup>[30]</sup> while as previously reported the incorporation of Zn ion into porphyrins causes alteration of the position of *meso*-substituents.<sup>[71]</sup>

As expected, the calculated transition energies of ZnP are degenerate and the rotational strengths are zero, which correspond to the orthogonal orientation of electric and magnetic dipole moments (Tables 1 and S1). The energies of orbitals involved into the electronic transitions of the B-region, calculated using the  $\omega$ B97X-D/cc-pVTZ and aug-cc-pVDZ basis sets, are similar and shown in Figures 2 and S1 and Table S2.

In agreement with the Gouterman's model the two LUMOs of ZnP are degenerate and the two HOMOs are "accidentally" degenerate.<sup>[118,119]</sup> As shown in Figures 2 and S1, all substituents increase the energy gap between HOMO and HOMO-1, on one hand and the energy gap between LUMO and LUMO+1, on the other hand. Herein, a clear tendency is observed as follows: the electron-donating substituents destabilize both HOMO and LUMO+1 (except for molecules containing Ph derivatives), while the electron-withdrawing groups lower the energy of both LUMOs and HOMOs (except ZnDP-F). As a result, the HOMO-LUMO gap increases along with increasing the electron-donating properties, in agreement with the observation of Ma et al.<sup>[73]</sup> Moreover, in the systems where the electronic commu-

nication or  $\pi$ -conjugation between porphyrin and the orthogonal substituents are prevented, LUMOs are more affected than HOMOs. This agrees with the previous studies.<sup>[41,46,70,112,120–124]</sup> In agreement with the observation of Theisen et al.<sup>[76]</sup> addition of the phenyl groups decreases the HOMO-LUMO gap as compared to the Ph free analogues. Subsequent introduction of different functional groups at the *p*-positions of Ph slightly destabilized HOMOs and increased the energy gap between HOMO and HOMO-1, however this influence was significantly smaller when compared to the effect caused by the substituents on a porphyrin ring (Table S2).

It should be noted that the *meso*-substituents influence both HOMOs, but their effect on the  $a_{1u}$  orbital is smaller, since this orbital has nodes at the *meso*-positions (Figures 2 and S2).<sup>[69,124–126]</sup> As was mentioned above, the electron-donating and electron-withdrawing substituents behaved oppositely to each other by destabilizing and stabilizing the  $a_{2u}$  orbital, respectively. In the case of CN and NO<sub>2</sub> substituents, the effect is so strong that it even causes inversion of the orbitals order with respect to other substituted porphyrins, which agrees with the observations of Walters *et al.*<sup>[69]</sup> and Liao *et al.*<sup>[124]</sup> Halogens having both electron-donating and electron-withdrawing characteristics, as was reported by Yamaguchi *et al.*<sup>[52]</sup> and Liao *et al.*,<sup>[124]</sup> stabilized the  $a_{1u}$  orbital and destabilize the  $a_{2u}$  orbital, as it was observed in ZnDP-F. In the case of Ph and its functionalized derivatives the inversion of LUMOs was found to take place (Figure S2).

Replacement of hydrogens with other substituents has a dual effect: destabilizes HOMO-1 and/or stabilizes LUMOs by removing the energy degeneracy of frontier orbitals, which in turn shifts the corresponding electronic transitions to a lower energy (Tables 1 and S1). The electron-donating substituents shifted the transition energy by 7–35 nm to the red region, while in the case of electron-withdrawing groups the low energy shift was noticeably smaller being 1–14 nm. This agrees with the previously obtained theoretical and experimental results, which showed that introduction of the peripheral substituents resulted in broaden<sup>[61,63,70]</sup> and red shifted<sup>[51,61,67,69]</sup> B-bands. Thus, Lee *et al.*<sup>[61]</sup> experimentally showed that in zinc porphyrins with  $\pi$ -conjugated electron-donating groups the B-bands are 5–14 nm red shifted depending on the reference complex. LeCours *et al.*<sup>[62]</sup> based on the absorption spectra reported that the energies of the B-bands of [5,15-bis[(aryl) ethynyl]-10,20-diphenyl-porphinato]zinc(II) complexes are up to 20 nm shifted to the lower energy region as compared to the complex with phenyl substituents. In different zinc porphyrins with various *meso*-substituents experimentally studied by Zawadzka *et al.*<sup>[35,127]</sup> the B-bands were shifted by 12–17 nm. Nowak-Król *et al.*<sup>[128]</sup> and Huang *et al.*<sup>[129]</sup> based on the experimental measurements also found that the B-bands in zinc porphyrins can be red-shifted up to 24 nm, depending on the *meso*-substituents. Magdaong *et al.*<sup>[130]</sup> observed the 12 nm difference between the B-bands absorption maxima of ZnP and ZnDPP in both PhCN and toluene that correlates well with our calculation result of 10 nm. Moreover, the electron-donating/withdrawing effects of functionalized Ph derivatives had a minor (about 1–2 nm) influence on the transition energies. This

**Table 1.** The maximal rotational strengths (R(v) of B electronic transitions, corresponding energies, and g-factors calculated for flat zinc porphyrins using  $\omega$ B97X-D/cc-pVTZ basis set.

Porphyrin	Excit.	Ex. en. [nm]	R(v) [cgs]	g-factor, $10^{-6}$
ZnDP-NMe <sub>2</sub>	V	383	-0.05	-0.12
	VI	382	0.31	0.95
ZnDP-C≡CPH-NMe <sub>2</sub> - <i>p</i>	III	402	2.21	3.88
	IV	398	-1.17	-5.30
ZnDP-C≡CPH-NO <sub>2</sub> - <i>p</i>	III	401	0.33	0.59
	IV	395	-0.17	-0.79
ZnDP-OC(O)H	III	380	0.09	0.27
	IV	379	0.85	2.10
ZnDPP-NMe- <i>p</i>	III	385	0.68	4.90
	IV	381	-0.05	-0.63



is also in line with the observation of Guberman-Pfeffer et al.,<sup>[58]</sup> which was based on the simulated absorption spectra, and reported that Ph vs Ph-CF<sub>3</sub>-*p* had no effect on the optical properties. This also correlated with the theoretical and experimental observation of Lebedev *et al.*<sup>[30]</sup> that *p*-methoxycarbonyl groups shifted the B-band by 4–5 nm to the red region as compared to free-base *meso*-tetrabenzoporphyrin, where the position of *meso*-groups are close to orthogonal.

In the case of substituted zinc porphyrins, the calculated rotational strengths become non-zero. Moreover, both the electron-donating and electron-withdrawing groups increased the absolute values of the calculated rotational strengths. This could be explained by minimal interference of the  $\pi$ - $\pi$  conjugation in the orbitals of peripheral substituents and porphyrin<sup>[76]</sup> or by in plane reorganization of the atoms,<sup>[30,112]</sup> which generates chirality in an inherently achiral zinc porphyrin. In Table 1 the Kuhn's *g*-factors (the dissymmetry or anisotropy factors), which are the ratio of ECD and absorbance signals, are given. The *g*-factors for the majority of studied systems are negligibly small being in the range of 10<sup>-6</sup>–10<sup>-7</sup>, but not zero, hence proving their asymmetry. However, the calculated values of the rotational strengths are essentially small. For all porphyrins except ZnDP-C≡C-Ph-NMe<sub>2</sub>-*p*, the absolute values of the rotational strength in the B-region are less than 1.0 cgs, and consequently, the ECD spectra of these porphyrins are experimentally undetectable. In the case of ZnDP-C≡C-Ph-NMe<sub>2</sub>-*p*, as the most distorted molecule, the calculated rotational strengths are 2.2 and -1.2 cgs. This agrees with the previously obtained experimental reports about silent ECD spectra of achiral porphyrins.<sup>[131,132]</sup>

In summary, incorporation of the electron-donating or electron-withdrawing groups removes the energy degeneracy of HOMOs and LUMOs and splits the excitation energies of the two B electronic transitions. However, in planar achiral porphyrins the orientation of electronic and magnetic transition moments remains orthogonal resulting in rotational strengths close to zero and subsequently silent ECD spectra.

### 2.3. Influence of Spatial Orientation of Porphyrin Peripheral Substituents

The total rotational strength has two types of major contributions: intrinsic rotational strength of the porphyrin electronic transitions and perturbations caused by coupling between the transitions of porphyrin and other chromophoric moieties.<sup>[94,95,117]</sup> As it was shown in investigations of Nagai et al.,<sup>[96]</sup> Kobayashi et al.<sup>[95]</sup> and Kiefl et al.<sup>[117]</sup> the presence and relative orientation of peripheral chromophoric substituents strongly influence the intensities and signs of the ECD bands. To estimate the degree of this effect, the porphyrin plane was constrained to be planar, while the relative orientation of the peripheral substituents was varied to form a tilt of 60° or 120° with respect to the porphyrin plane with both mutual conrotatory and disrotatory relative orientations (Figure 3). In order to estimate a maximal potential influence of the orientation of the peripheral substituents, the dihedral angles

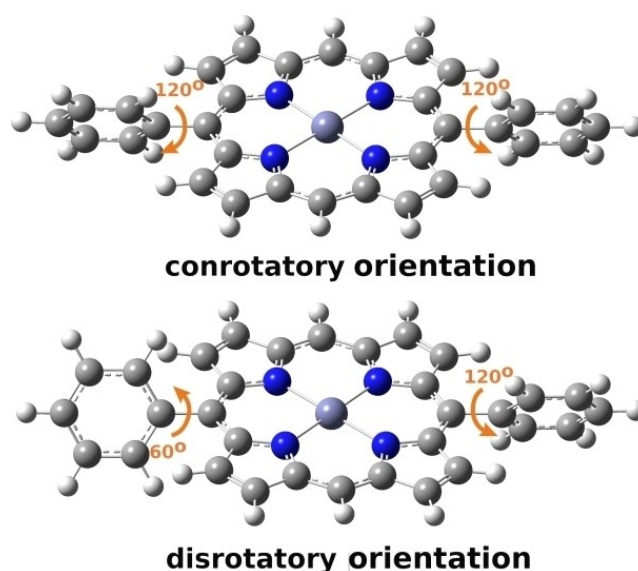
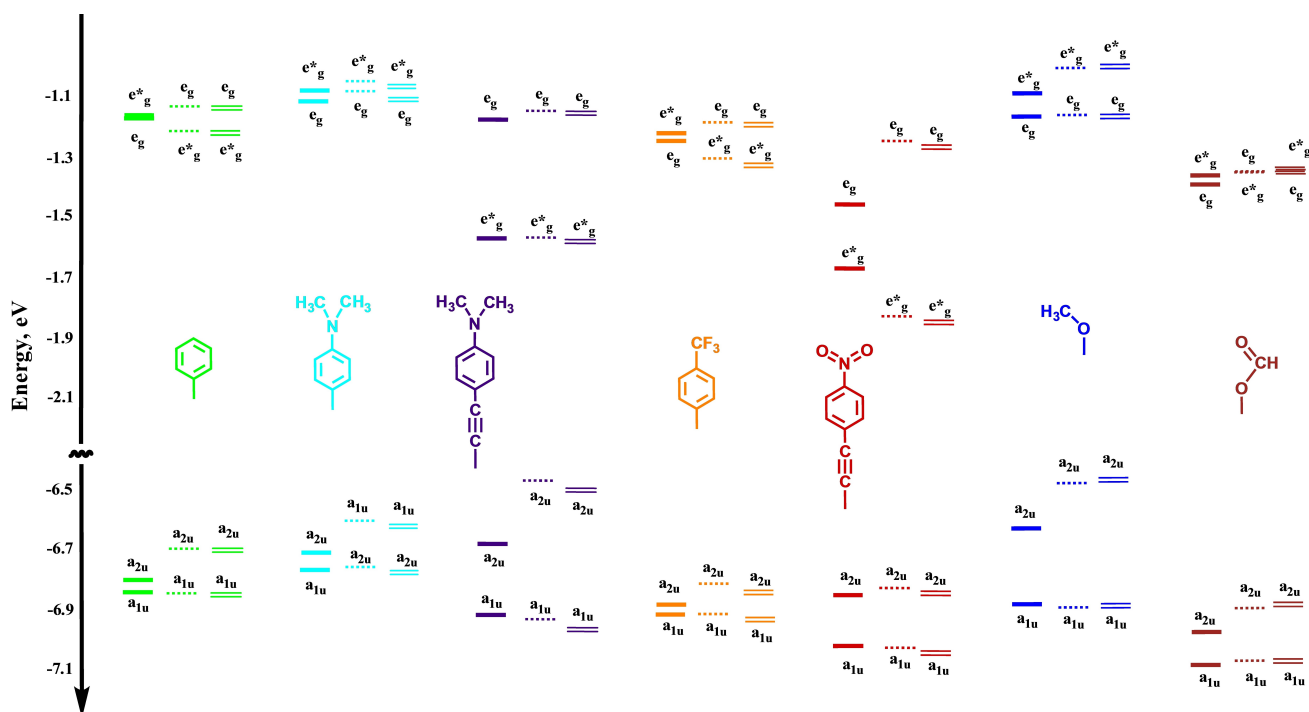


Figure 3. Spatial orientation of peripheral chromophoric substituents.

were chosen to be 60° and 120° being slightly smaller or larger than the standard dihedral angles in metal porphyrins in the ground state which are in the range of 69°–90° and 90°–111°, correspondingly.<sup>[51,71]</sup>

Similarly to previously discussed flat porphyrins, both HOMOs and LUMOs are sensitive to the spatial orientation of the peripheral substituents (Figures 4 and S3 and Table S3). The tilt of the peripheral substituents increases the energy gap between HOMO and HOMO-1 by destabilizing HOMO, whereas the energy of HOMO-1 remained almost unchanged. The tilt of the peripheral substituents also increases the energy gap between LUMOs by raising the energy of LUMO+1. The influence of the position of the substituents on the energies of the frontier orbitals could be rationalized by enhanced resonance and/or electronic communication and between the porphyrin ring and the substituents, together with increased electron density on the substituents (Figure S4).<sup>[61,69,70,133]</sup> In addition, for both HOMOs and LUMOs an inversion of orbitals was also observed (Figures 4, S3 and S4).

In all the examined porphyrins, the tilt of the peripheral substituents significantly changes the energies of frontier orbitals, which lead to a shift in the transition energies by up to 17 nm to the low energy region and an increase in the energy gap between the transitions by up to 12 nm (Tables 2 and S4). Thus, the smallest change in the energy gap between the electronic transitions was found for ZnDP-OMe and for ZnDP-OC(O)H. Noticeably, OMe is not a secondary chromophore and OC(O)H is a very weak secondary chromophore. In contrast, the largest energy gap between the electronic transitions was observed in the case of ZnDPP-NMe<sub>2</sub>-*p*, ZnDP-NO<sub>2</sub>, ZnDP-C≡C-Ph-NMe<sub>2</sub>-*p*, and ZnDP-C≡C-Ph-NO<sub>2</sub>-*p*. Apparently, this is because of the fact that these porphyrins have comparably strong secondary chromophores possessing a good electronic communication with the porphyrin ring. Also, a relative orientation of the peripheral substituents does not play



**Figure 4.** Energies of the orbitals involved into electronic transitions of flat ZnDPP, ZnDPP-NMe<sub>2</sub>-*p*, ZnDP-C≡C-Ph-NMe<sub>2</sub>-*p*, ZnDPP-CF<sub>3</sub>-*p*, ZnDP-C≡C-Ph-NO<sub>2</sub>-*p*, ZnDP-OMe and ZnDP-OC(O)H porphyrins calculated using ωB97X-D/cc-pVTZ. Solid lines–porphyrins with the orthogonal position of substituents; dashed lines–porphyrins with the conrotatory orientation of substituents; double lines–porphyrins with the disrotatory orientation of substituents.

**Table 2.** Energies, rotational strengths (R(v) of the B electronic transitions (III and IV) and g-factors in flat ZnDP-OC(O)H, ZnDP-OMe, ZnDP-C≡C-Ph-NMe<sub>2</sub>-*p*, ZnDP-C≡C-Ph-NO<sub>2</sub>-*p*, ZnDP-NO<sub>2</sub>, ZnDP-NMe<sub>2</sub> and ZnDPP-NMe<sub>2</sub>-*p* with substituents in the conrotatory and disrotatory orientation calculated using ωB97X-D/cc-pVTZ.

Porphyrin	Excit.	conrotatory orientation of Sub.			disrotatory orientation of Sub		
		Ex. en. [nm]	R(v) [cgs]	g-factor, 10 <sup>-5</sup>	Ex. en. [nm]	R(v) [cgs]	g-factor, 10 <sup>-5</sup>
ZnDP-OC(O)H	III	381	-0.02	-0.01	381	22.98	5.52
	IV	379	1.01	0.06	379	-2.14	-0.65
ZnDP-OMe	III	384	-0.07	-0.02	384	0.67	0.24
	IV	383	-0.06	-0.02	383	16.07	4.45
Zn-DP-C≡C-Ph-NMe <sub>2</sub> - <i>p</i>	III	417	-0.11	-0.02	417	49.38	11.05
	IV	405	0.03	0.02	405	-52.12	-29.75
ZnDP-C≡C-Ph-NO <sub>2</sub> - <i>p</i>	III	409	-0.05	-0.01	409	60.41	12.61
	IV	398	-0.02	-0.01	398	-56.70	-32.22
ZnDP-NO <sub>2</sub>	III	388	-0.19	-0.07	386	-158.11	-48.32
	IV	376	0.15	0.08	376	-37.87	-16.49
ZnDP-NMe <sub>2</sub>	III	406	2.86	0.87	406	135.86	44.41
	IV	403	0.95	0.44	403	-24.84	-11.66
ZnDPP-NMe <sub>2</sub> - <i>p</i>	III	402	0.24	0.06	402	-9.47	-2.15
	IV	391	-1.55	-0.77	391	-2.85	-1.42

a significant role as illustrated by an almost invariant energy gap between two electronic transitions in the same porphyrin for both conrotatory and disrotatory orientations of the peripheral substituents. This is in agreement with the experimental observations by Walters et al.,<sup>[69]</sup> that the difference in absorption energies of ZnTPP and ZnTPP-*X-p*, in which the positions of aryls usually deviate from the orthogonal orientation, can cause absorption shift up to 17–19 nm.<sup>[51,71]</sup> Also, the theoretical and experimental studies by Mizutani et al.<sup>[134,135]</sup> revealed that the supramolecules possessing hydrogen bonds, which prevent free rotation of the naphthyl substituents and

keep it in the tilt position, exhibited the ECD bands shifted by 3–6 nm to the lower energy region as compared to similar supramolecules without corresponding hydrogen bonds. Furthermore, the peripheral chromophoric *meso*-substituents themselves induced the red shifts by 17 nm.

As it was mentioned above, in the case of flat porphyrins with orthogonal peripheral substituents the calculated rotational strengths were close to zero. However, deviation of the peripheral substituents from the orthogonal position allows coupling between the porphyrin and secondary chromophore's π-π\* electronic transitions. It also should be noted that the tilt

of the substituents causes delocalization of the frontier orbitals (Figures 5 and S4). This results in increasing the asymmetry of modelled systems (greater g-factors), in a nonzero scalar product of electric and magnetic dipole moments and absolute values of rotational strengths of up to 158.1 cgs (Tables 2 and S4). In contrast to the excitation energies, the orientation of peripheral substituents is essential for the intensities. In most cases, when the peripheral substituents are in the conrotatory position, the rotational strength remains small (up to 2.86 cgs, 3.33 cgs using aug-cc-pVDZ basis set). The rotational strengths calculated using both cc-pVTZ and aug-cc-pVDZ are very similar and follow the same trend. However, although in the case of a conrotatory orientation of peripheral substituents the intensities are larger as compared to those of flat porphyrins with the orthogonal substituents, they are still relatively small to be observed experimentally. In Figure 6, the three most intensive ECD spectra obtained for ZnDPP–CF<sub>3</sub>-*p*, ZnDP–NMe<sub>2</sub> and ZnDP–OC(O)H are shown, while the ECD spectra of other porphyrins are shown in the Figure S5.

When the peripheral substituents are in a disrotatory orientation, the absolute values of the rotational strengths significantly increase (up to 158.1 cgs). The increase of the absolute values of the rotational strengths was observed in all the studied porphyrins, as a result of greater chirality generation (larger g-factors) (Tables 2 and S4). This agrees with the theoretical and experimental results obtained by Nagai et al.<sup>[96]</sup>

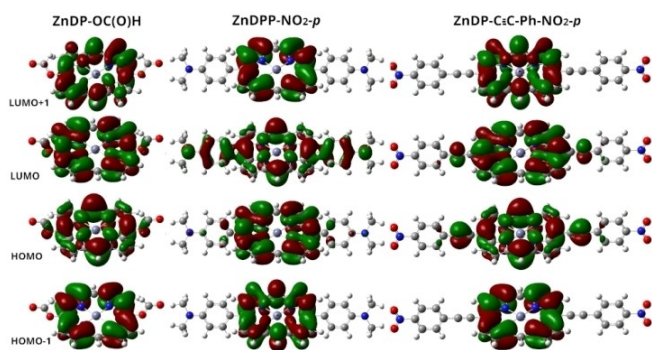


**Figure 5.** Frontier orbitals of ZnDP–OC(O)H, ZnDPP–NMe<sub>2</sub>-*p* and ZnDP–C≡C–Ph–NO<sub>2</sub>-*p*, with conrotatory orientation of peripheral substituents.

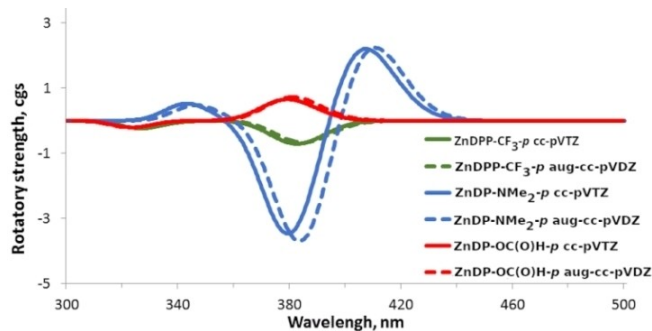


**Figure 6.** The most intensive ECD spectra of planar porphyrins

and Kobayashi et al.,<sup>[95]</sup> which showed that the relative orientation of chromophoric substituents influence the intensity and signs of corresponding ECD bands. Thus, in Figure 7a the four most intense ECD spectra are shown. Based on these data it could be concluded that the basis set used for simulation has a minor effect on the intense ECD spectra.

However, when the ECD signals are moderate (10–20 cgs), a clear dependence on the basis set is observed (Figures 7b and S6 and Table S4). It was found that varying the basis set changes not only the intensity of the peaks (ZnDPP–CF<sub>3</sub>-*p* and ZnDPP–NMe<sub>2</sub>-*p*), but also the sign (ZnDPP, ZnDP–OC(O)H, ZnDPP–Me-*p*, and ZnDPP–OMe-*p*). Wherein, the rotational strengths calculated using the length and velocity formalisms differ by 0.02–0.90 and 0.4–1.7 cgs for the cc-pVTZ and aug-cc-pVDZ basis sets, respectively. In previous theoretical works<sup>[136,137]</sup> these differences were considered as small and it was concluded that the size of both basis sets is enough for a good description of the electric dipole moments.

In summary, the tilt of the peripheral substituents increases the energy gap between the two B electronic transitions and shifts them to a lower-energy region. However, the position of the substituents relative to each other is not so significant for the transition energies, but essential for the rotational strengths. The observed tendency in increasing the absolute value of rotational strengths is in the following order of

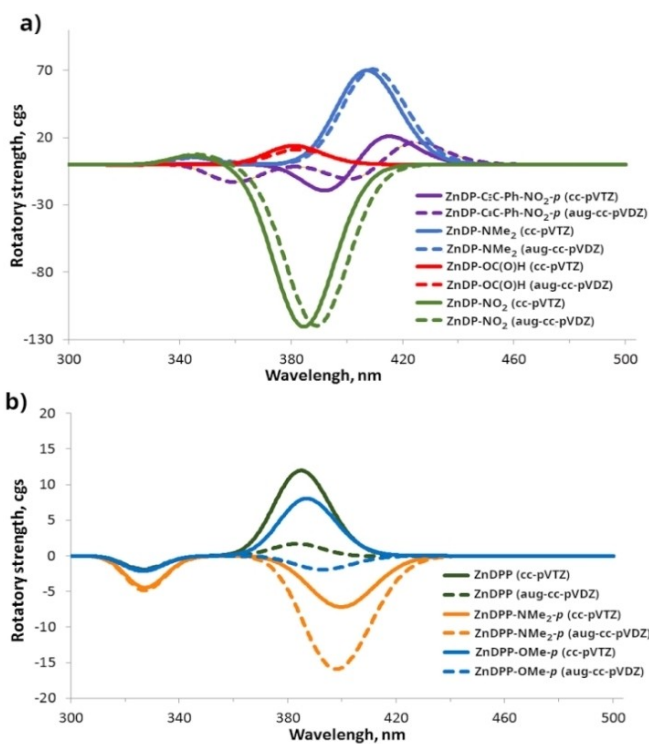


**Figure 7.** a) The most intensive ECD spectra of planar porphyrins (ZnDP–C≡C–Ph–NO<sub>2</sub>-*p*, ZnDP–NMe<sub>2</sub>, ZnDP–OC(O)H and ZnDPP–NO<sub>2</sub>) with the disrotatory orientation of peripheral substituents and b) moderate ECD spectra of planar porphyrins (ZnDPP, ZnDPP–NMe<sub>2</sub>-*p*, and ZnDPP–OMe-*p*) with the disrotatory orientation of peripheral substituents simulated using the ωB97X-D functional, cc-pVTZ (solid line) and aug-cc-pVDZ (dashed line) basis sets.

substituent orientation: orthogonal > conrotatory orientation > disrotatory orientation. In principle, if the peripheral substituents are fixed in a certain orientation they will have significant impact on induced chirality, and hence on the intensity of the ECD bands. In addition, the corresponding ECD signals will be shifted to the low energy region.

## 2.4. Influence of Porphyrin Plane Distortion

In general, the porphyrin plane is flexible<sup>[138–142]</sup> and relatively modest energies of  $10.2 \text{ kcal mol}^{-1}$  are required for the out of plane deformation of a free base porphyrin.<sup>[143]</sup> The deformations can occur as a result of the influence of the environment,<sup>[60,144,145]</sup> bulky substituents,<sup>[32,47–52,146]</sup> and complexation of an axial ligand.<sup>[98,139,147]</sup> Apparently, the out of plane deformations weaken the macrocycle  $\pi$ -electronic system

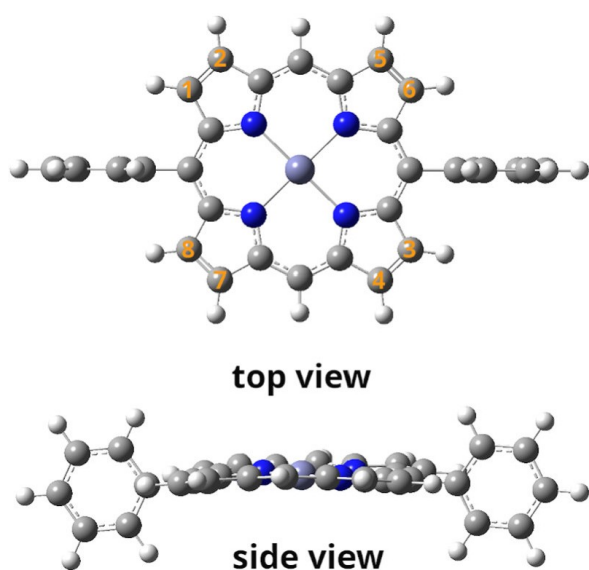


Figure 8. Distortion of porphyrin plane.

through reducing the overlap of neighboring  $p_z$  orbitals,<sup>[138]</sup> and hence may generate chirality in achiral porphyrins. Therefore, in this particular case the structural changes are strongly correlated with the intrinsic rotational strength<sup>[42,58,117]</sup> and are also a main factor responsible for the low energy shift of B-band.<sup>[55,147]</sup> However, Pfeffer et al.<sup>[58]</sup> stated that, although non-planarity is the main factor which influences absorption spectra, it is not the only one. In contrast Cramariuc et al.<sup>[51]</sup> reported that distortion by its own covers less than 20% of the HOMO-LUMO energy gap decrease.

In order to investigate the role of the structural deformation, the porphyrin planes were distorted so that the dihedral angles between two  $C_\beta$  of one pyrrole ring and between two  $C_\beta$  of the diametrically opposite pyrrole ring were  $4^\circ$ ,  $8^\circ$ , and  $12^\circ$  (for  $C_1-C_2-C_3-C_4$ ) or  $-4^\circ$ ,  $-8^\circ$ , and  $-12^\circ$  (for  $C_5-C_6-C_7-C_8$ ), respectively (Figure 8). The corresponding pairs of these angles were frozen and the peripheral aromatic substituents were fixed in the perpendicular position to the porphyrin plane during geometry optimization in order to decrease coupling between the dipole moments of porphyrin and substituent.

According to the observations of Zhou et al.<sup>[57]</sup> and Zhang et al.<sup>[86]</sup> the structural distortion of porphyrin plane destabilizes HOMOs and LUMOs, but in the porphyrins studied here the destabilization was found to be relatively small, up to 0.07 or 0.11 eV using cc-pVTZ and aug-cc-pVDZ basis sets, respectively (Table S5). Thus, the orbital energies change is smaller than that in the case of introduction and orientation variability of the peripheral substituents. The energy gaps between the orbitals are also not changed significantly with the transition energies remained close to each other (Tables 3 and S6). This agrees with the results of Cramariuc et al.<sup>[51]</sup> that distortion by its own covers less than 20% of the HOMO-LUMO energy gap decrease, and disagrees with the previous experimental researches stating that the porphyrin plane distortion leads to lower absorption energy.<sup>[49,52,57]</sup> We suggest that this is a result of exclusion of dynamic and solvent effects and coupling between porphyrin and peripheral chromophoric substituents.

Table 3. Most intense rotational strengths  $R(v)$  of the B electronic transitions (III and IV), energies correspond to them and g-factors in distorted porphyrins calculated using  $\omega$ B97X-D/cc-pVTZ.

Porphyrin	Excit.	Distortion at $4^\circ$			Distortion at $8^\circ$			Distortion at $12^\circ$		
		Ex. en. [nm]	$R(v)$ [cgs]	g-factor, $10^{-5}$	Ex. en. [nm]	$R(v)$ [cgs]	g-factor, $10^{-5}$	Ex. en. [nm]	$R(v)$ [cgs]	g-factor, $10^{-5}$
ZnP	III	372	<b>-44.06</b>	-12.23	372	-14.91	-4.15	373	5.50	1.54
	IV	372	<b>44.12</b>	12.25	372	14.95	4.16	373	-5.48	-1.53
ZnDP-C $\equiv$ C-Ph-NO $_2$ -p	III	401	<b>-5.26</b>	-0.96	401	-5.26	-0.96	402	-0.71	-0.13
	IV	395	<b>3.92</b>	1.78	395	3.55	1.61	396	0.27	0.12
ZnDP-NO $_2$	III	376	<b>6.32</b>	1.63	376	-1.62	-0.42	376	0.46	0.12
	IV	374	<b>-0.74</b>	-0.23	374	0.68	0.21	374	0.00	0.00
	V	366	<b>-4.11</b>	-684.93	366	0.78	29.17	366	2.52	96.98
ZnDP-CF $_3$	VI	366	<b>-0.64</b>	-858.80	366	0.02	3.68	366	<b>-2.83</b>	-97.68
	III	375	<b>22.57</b>	5.72	377	-0.22	-0.06	377	0.16	0.04
	IV	370	<b>-17.21</b>	-6.00	372	0.16	0.09	373	-0.10	-0.04
ZnDPP-Me-p	V	349	<b>-8.45</b>	-4225.30	353	0.02	2.67	354	-0.04	-1627
	III	383	-6.42	-1.51	384	<b>-15.25</b>	-3.56	384	-3.06	-0.72
	IV	381	4.87	1.94	381	<b>11.77</b>	4.70	381	2.39	0.96
ZnDPP-CF $_3$ -p	III	383	-0.68	-0.16	383	<b>-15.19</b>	-3.63	384	-0.02	0.00
	IV	380	0.58	0.23	381	<b>12.03</b>	4.80	381	0.07	0.03



Despite of a small influence on the transition energies, distortion of the porphyrin plane has a significant effect on the corresponding rotational strengths (Tables 3 and S6, with the largest values highlighted in bold). Furthermore, it influences the corresponding *g*-factors, which became larger than those of flat porphyrins with the conrotatory orientation of substituents, but still being smaller than the *g*-factors of flat porphyrins with the disrotatory orientation of the substituents. The largest calculated absolute values of the rotational strengths (*ca.* 44 cgs) correspond to ZnP, when the twist angles of opposite pyrrole rings were 4°. However, this value was further decreased down to 5.5 cgs with increasing the distortion to 12°. In the case of other distorted porphyrins, the rotational strength was significantly smaller because of electronic communication and coupling with the peripheral substituents. For example, for non-aromatic and non-planar substituents (such as NMe<sub>2</sub>, OMe, NO<sub>2</sub>, CF<sub>3</sub>) the maximum absolute values of rotational strength also corresponded to the distortion of 4° and varied from 1.4 cgs for OMe to 22.6 cgs for CF<sub>3</sub>. In contrast, in the case of linear substituents (such as F and CN) the absolute values of rotational strengths increased insignificantly upon distortion and did not exceed 0.1 cgs. A similar situation was observed for Me, Ph, Ph–NMe<sub>2</sub>-*p*, where the absolute values of rotational strengths increased up to 0.5 cgs with distortion. For other aromatic substituents, the largest absolute values of the rotational strength could be observed at different degrees of porphyrin distortion. For example, the maximum absolute value of ZnDPP–CF<sub>3</sub>-*p* (15.1 cgs) was observed at 8°, while ZnDPP–C≡C–Ph–NMe<sub>2</sub>-*p* has rotational strengths of 4.3 and 4.1 cgs at 4° and 12°, respectively. This agrees well with the conclusion by Graves et al.<sup>[60]</sup> based on the experimental and theoretical study of heme about a nonlinear absorption dependence upon distortion.

As the rotational strength is a scalar product of the transition electric and magnetic dipole moments, an angle of 90° between these two vectors results in zero rotational strength. Hence, in general the larger deviation from 90° subsequently yields the greater absolute value of rotational strength that was corroborated by the obtained results. However, in ZnDPP–Me-*p*, ZnDP–C≡C–Ph–NMe<sub>2</sub>-*p*, and ZnDP–C≡C–Ph–NO<sub>2</sub>-*p* the decrease in deviation was compensated by a significant increase in the transition magnetic dipole moments. This is because of enlargement of the deformation of the porphyrin plane, which led to increase of the transition magnetic dipole moments by several orders of magnitude, whilst the transition electric dipole moments remained almost unchanged (see, Table S7, with the largest values highlighted in bold). The results obtained using the aug-cc-pVDZ basis set were close to those using cc-pVTZ (see, Table S7). However, it should be noticed that in contrast to the transition electric dipole moments, the magnetic dipole moments are not invariant in present calculations.

As has just been shown, whilst the distortion of the porphyrin plane plays a significant role in the appearance of the ECD signals, this is not the sole factor to be considered. This observation agrees well with the previously mentioned conclusion of Guberman-Pfeffer et al.<sup>[58]</sup> and Cramariuc et al.<sup>[51]</sup> that

non-planarity is partly responsible for the observed shift. In spite of the fact that distorted ZnP has the largest calculated absolute values of rotational strengths, because of their degeneracy and opposite signs, they could not be observed in experimental ECD spectra (Table S6 and Figures 9 and S7). This is also in agreement with the experimentally observed silent ECD spectra of non-ligated distorted porphyrins.<sup>[148,149]</sup>

In the most distorted porphyrins the absolute values of the rotational strengths were smaller than 1.0 cgs, too small to be observed experimentally. In the case of ZnDPP–Me-*p*, ZnDPP–CF<sub>3</sub>-*p*, and ZnDP–CF<sub>3</sub> the bisignate B-band with less intensive higher-energy component was simulated (Figures 9a and S7). In the case of ZnDP–NMe<sub>2</sub>, ZnDP–NO<sub>2</sub>, ZnDP–C≡C–Ph–NMe<sub>2</sub>-*p*, and ZnDP–C≡C–Ph–NO<sub>2</sub>-*p*, the substituents and further distortion of porphyrin plane led to stabilization of LUMO+2 and LUMO+3 (ZnDP–NMe<sub>2</sub> and ZnDP–NO<sub>2</sub>) or destabilization of HOMO-2 and HOMO-3 (ZnDP–C≡C–Ph–NMe<sub>2</sub>-*p* and ZnDP–C≡C–Ph–NO<sub>2</sub>-*p*) yielding additional transitions in the B-band region and its bisignate profile (Figures 9b and S7). As seen in Figure 9b, the ECD spectra of ZnDP–NMe<sub>2</sub> exhibit the most intense bands when the porphyrin plane is distorted by 4°. Furthermore, upon increasing the distortion up to 8° the signals intensities are decreased and the signs are inverted.

In summary, deformation of the porphyrin plane does not affect the excitation energies, but has a significant impact on the rotational strengths and changes not only its absolute value but also is able to switch an ECD sign. Furthermore, coupling

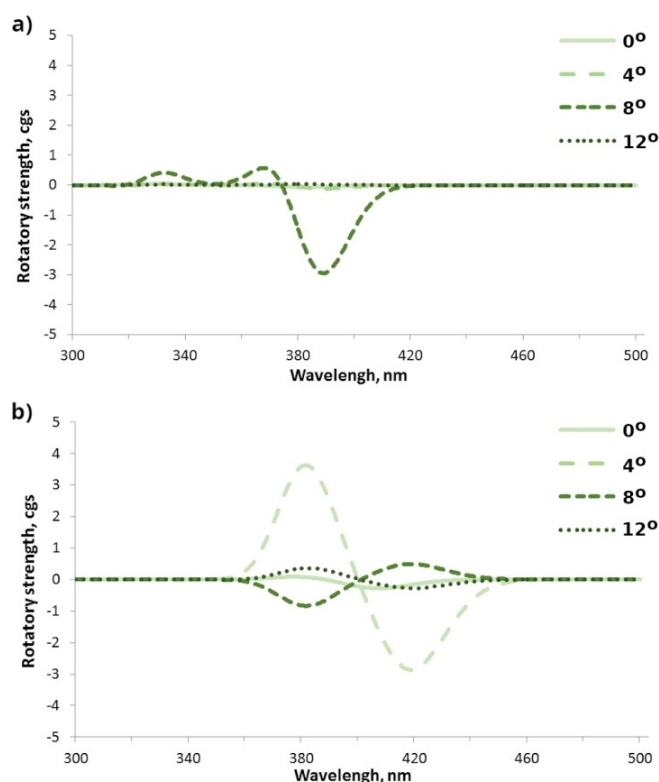


**Figure 9.** Simulated ECD spectra of distorted a) ZnDPP–CF<sub>3</sub>-*p* and b) ZnDP–NMe<sub>2</sub> calculated using ωB97X-D/cc-pVTZ.

**Table 4.** The maximal rotational strengths  $R(v)$  of B electronic transitions (III and IV) corresponding energies and g-factors calculated for axially ligated flat porphyrins and fully optimized axially ligated porphyrins using  $\omega$ B97X-D/cc-pVTZ.

Porphyrin	Excitat.	Flat ligated porph.			Fully opt. ligated porph		
		Ex. en. [nm]	$R(v)$ [cgs]	g-factor, $10^{-4}$	Ex. en. [nm]	$R(v)$ [cgs]	g-factor, $10^{-4}$
ZnDP-OC(O)H	III	393	-39.4	-4.17	393	-18.2	-1.91
	IV	391	31.7	2.78	392	7.3	0.64
ZnDP-NO <sub>2</sub>	III	390	-2.8	-0.27	400	122.5	13.35
	IV	389	15.8	1.80	394	-0.4	-0.07
ZnDP-CF <sub>3</sub>	III	388	16.1	1.81	391	-151.9	-17.41
	IV	387	-18.7	-2.79	389	132.2	20.19
ZnDPP-Me- <i>p</i>	III	397	-35.9	-2.69	400	2.5	0.19
	IV	395	18.9	2.27	397	-2.3	-0.32
ZnDPP-NMe <sub>2</sub> - <i>p</i>	III	398	-4.9	-0.36	409	39.9	2.81
	IV	395	-5.1	-0.71	401	-29.4	-4.82

between the electronic transition moments of the porphyrin unit and the peripheral aromatic substituents decreases the absolute values of rotational strengths. In contrast to the previous experimental statements,<sup>[32,47–50]</sup> it was found that the symmetrical deformation of a porphyrin plane does not shift the ECD bands to the low energy region, while it can influence its sign and intensity.

## 2.5. Influence of Axial Ligation

It is well known that in five-coordinative complexes, an axial ligand causes a displacement of the metal ion out of the porphyrin core<sup>[85,139,140]</sup> and also distorts the plane of the macrocycle,<sup>[44,57,85–90]</sup> hence causing the porphyrin ring contraction.<sup>[44,86]</sup> Moreover, axial ligation changes the energies and shapes of the frontier orbitals.<sup>[80,85,86]</sup> ECD spectra are

sensitive to both electronic and geometric factors, which are altered by ligand binding.<sup>[41,79,86,96,150,151]</sup> As a result of these perturbations, the excitation energies of ligated metal porphyrins are shifted to low<sup>[41,44,79,86,96,152]</sup> or high<sup>[92]</sup> energy. For zinc porphyrins the ligation causes a red shift.<sup>[91,92,153]</sup> In addition, upon axial ligation the B electronic transitions acquire a charge transfer character.<sup>[41,99]</sup>

In order to understand how axial ligation influences the corresponding electronic transitions and subsequently the ECD spectra without any geometry changes, we simulated the spectra of flat ligated porphyrins, where the peripheral chromophoric substituents were fixed perpendicularly to the macrocycle plane (Figure 10).

In agreement with the previous theoretical and experimental studies,<sup>[80,85,86]</sup> binding of an axial ligand to flat porphyrins destabilizes both HOMOs and to a smaller extent both LUMOs (Figures 11 and S8 and Table S8). In porphyrins with electron-donating substituents, the axial ligation increases the energy gaps between HOMO and HOMO-1 as well as between LUMO and LUMO+1, hence removing the degeneracy of the frontier orbitals. It also decreases the HOMO-LUMO gap. In the case of porphyrins with electron-withdrawing substituents, axial ligation increases the energy gaps between HOMO and HOMO-1 (except ZnDP-CF<sub>3</sub>, ZnDP-CN and ZnDP-NO<sub>2</sub>, where in ligated complexes the inversion of HOMO and HOMO-1 relative to the same non-ligated complexes or ligated ZnP took place), but the energy gap between LUMO and LUMO+1 remains the same. The energies of the orbitals involved in the electronic transitions in the B absorption region calculated using the aug-cc-pVDZ basis set are similar to those obtained using the cc-pVTZ basis set (Table S8). It was found that axial ligation shifted the transition energies to the low energy region by about 10–19 nm (Tables 4 and S9), in agreement with the experimentally measured values of 10.4 nm reported by Kolling et al.<sup>[91]</sup> and 15.4 nm reported by Nappa et al.<sup>[153]</sup> Our results also agree with the experimental observations by Walters et al.<sup>[69]</sup> that *para* substituents on Ph shift the transition energies up to 17 nm to lower energy.

Moreover, in all cases, except ZnDP-NMe<sub>2</sub>, the energy gap between the third and fourth transitions is increased by about 1–12 nm as compared to the ligand free flat porphyrin. In flat ligated ZnDP-NMe<sub>2</sub>, ZnDP-NO<sub>2</sub>, ZnDP-CN, ZnDP-CF<sub>3</sub>,

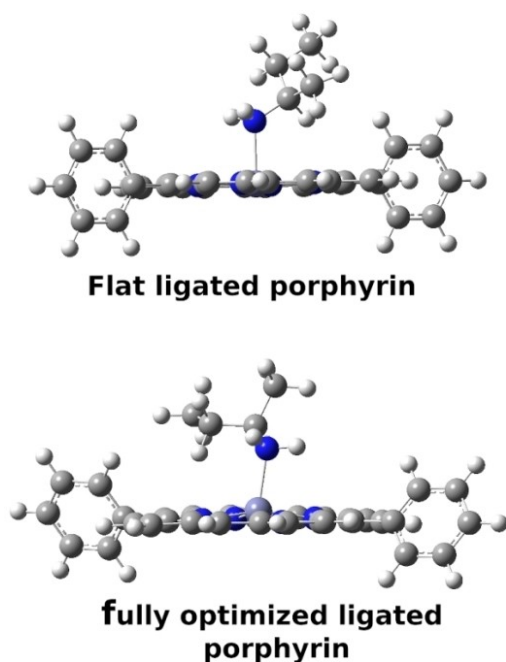


**Figure 10.** Ligated porphyrins.

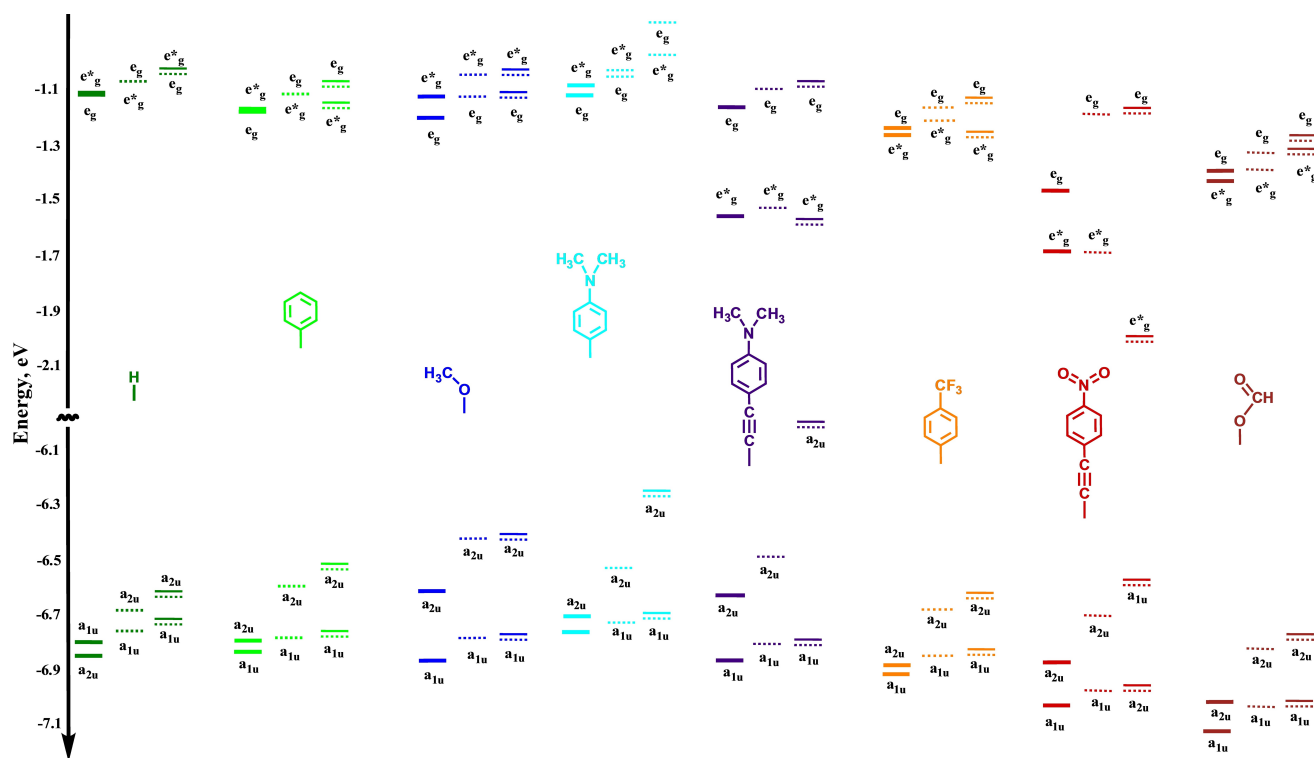


**Figure 11.** Energies of orbitals involved into the electronic transitions of ZnP, ZnDPP, ZnDP-OMe, ZnDP-NMe<sub>2</sub>-p, ZnDP-C≡C-Ph-NMe<sub>2</sub>-p, ZnDPP-CF<sub>3</sub>-p, ZnDP-C≡C-Ph-NO<sub>2</sub>-p, ZnDP-OC(O)H porphyrins calculated using ωB97X-D/cc-pVTZ. Solid lines–flat non ligated porphyrins; dashed lines–flat ligated porphyrins; double lines–fully optimized ligated porphyrins.

ZnDP-C≡C-Ph-NMe<sub>2</sub>-p and ZnDP-C≡C-Pp-NO<sub>2</sub>-p, transitions with a large contribution of the transition from the lowest HOMO-X, close in energy to HOMO-1, were observed in the B region (Tables S9 and S10). The transitions from the lowest HOMO-X also explain the constant nature of the energy gap between the third and the fourth transitions in ZnDP-NMe<sub>2</sub> upon axial ligation. In contrast to all other studied flat porphyrin complexes, in flat ligated ZnDP-NMe<sub>2</sub> the third and fourth transitions are transitions from substituent-localized HOMO-2 or HOMO-3 to LUMO or LUMO + 2 that is similar to flat non-ligated ZnDP-NMe<sub>2</sub> (Figure 12).

Axial ligation also influences the rotational strengths by significant enhancement of its absolute values. Herein, it should be noted that the electric transition moments are almost unchanged (Table S11a). This enhancement may relate to increasing the angle deviation between the corresponding electric and magnetic dipole moments from 90° (for non-ligated porphyrins) by 1–2° (for flat ligated porphyrins), and to enlarging the magnetic transition moments by 1–2 orders of magnitude as compared to ligand free flat porphyrins, the magnetic dipole moments of which are close to zero (Table S11). However, in contrast to the transition electric dipole moments, the magnetic dipole moments are not invariant in the present calculations. Flat ligated ZnDP-C≡C-Ph-NMe<sub>2</sub>-p and ZnDP-C≡C-Ph-NO<sub>2</sub>-p behaved differently. Due to strong electron communication, a significant change in the transitions electric dipole moments upon complexation was observed.

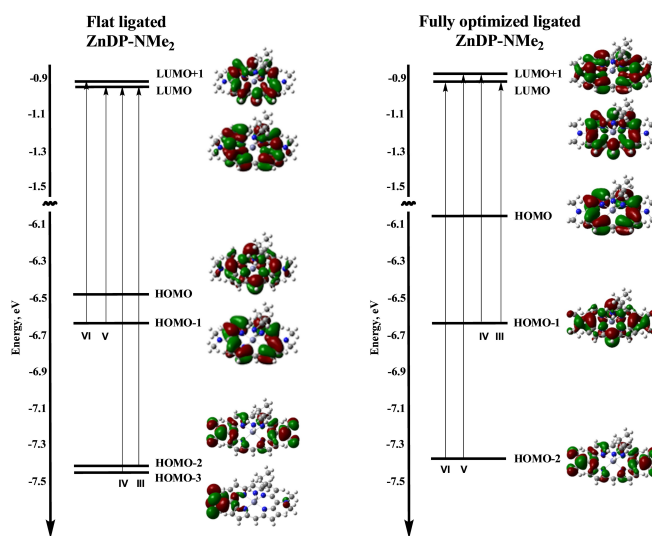


**Figure 12.** Frontier orbitals of ligated ZnDP-NMe<sub>2</sub> involved in the B transitions, showed the most intensive transitions.

Also, the g-factors of ligated porphyrins increased by 1–2 orders of magnitude as compared to non-ligated porphyrins, hence indicating asymmetry generation upon binding a chiral ligand. However, the guest studied in the present work does not significantly distort the porphyrin plane either interact with the peripheral substituents, which significantly decrease the

calculated g-factor as compared to the real-life systems having the corresponding g-factor values in the range of  $+/-10^{-5}-10^{-2}$ .<sup>[154]</sup>

The ECD spectra simulated using the cc-pVTZ basis set (Figure S9) are similar to those simulated using the aug-cc-pVDZ basis set. In the cases of flat ligated porphyrins (ZnP, ZnDPP-Me-*p*, ZnDPP-NMe<sub>2</sub>-*p*, ZnDPP-OMe-*p*, ZnDP-OMe, ZnDP-OC(O)H, ZnDP-Me, ZnDP-F) one negative band of 5–10 cgs is obtained (Figures 13 and S9). In flat ligated ZnDP-C≡C-Ph-NMe<sub>2</sub>-*p* and ZnDP-C≡C-Ph-NO<sub>2</sub>-*p* the ECD bands were also negative but with lower intensity (Figure S9). In flat ligated ZnDP-CF<sub>3</sub> two closely located negative bands were found (Figure 13b). In the case of flat ligated ZnDPP and ZnDPP-CF<sub>3</sub>-*p* the ECD bands were also positive (Figures 13a and S9). In flat ligated ZnDP-CN, ZnDP-CF<sub>3</sub> and ZnDP-NO<sub>2</sub>

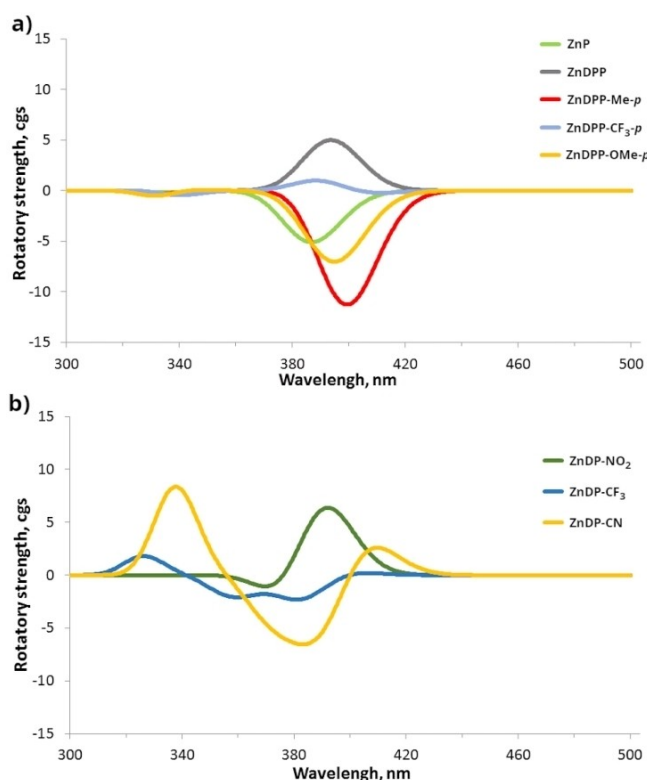


Figure 13. ECD spectra of flat ligated porphyrins a) ZnP, ZnDPP,

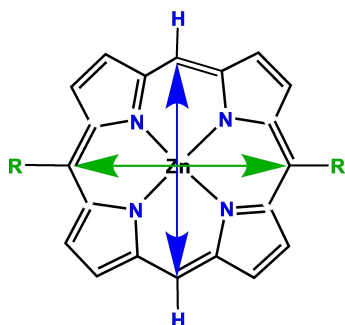


Figure 14. Contraction of the porphyrin core caused by ligation.

two/three peaks of opposite signs in the B-band region were observed because of presence of the corresponding third/fourth transition (Figure 13b).

However, as it was previously reported, binding an axial ligand causes a distortion of the porphyrin ring,<sup>[98,99]</sup> displacement of the metal ion out of the macrocycle plane,<sup>[85,139,140]</sup> and consequent contraction of the porphyrin core.<sup>[44,86]</sup> In the studied fully optimized complexes upon axial ligation both the corresponding porphyrin distortion of *ca* 1–3° and metal ion displacement were observed (Table S12). This resulted in lengthening of the C<sub>meso</sub>-C'<sub>meso</sub> (C<sub>meso</sub>-R) distances by about 0.005–0.1 Å, while other C<sub>meso</sub>-C'<sub>meso</sub> (C<sub>meso</sub>-H) shortened (green and blue arrows in Figure 14). The maximal and minimal C<sub>meso</sub>-C'<sub>meso</sub> (C<sub>meso</sub>-R) changes of distances are 0.222 and 0.001 Å for ZnDP-Me and ZnP, respectively.

By analogy with flat axially ligated porphyrins, axial ligation in fully optimized porphyrins destabilizes both HOMOs and one or both LUMOs (Figures 11, S8 and Table S13), with LUMOs being destabilized to a lesser extent. In the majority of fully optimized host-guest complexes the energy gaps between HOMO/HOMO-1 and between LUMO/LUMO+1 increase as compared to flat axially ligated porphyrins, thus decreasing the overall HOMO-LUMO gaps. Interestingly, in flat and fully optimized ligated porphyrins the electron density of the frontier orbitals was mainly localized on the porphyrin plane and partly on the peripheral substituents and on nitrogen of the guest (Figures S10 and S11).

Axial ligation shifts the transition energies to the red region up to 26 nm as compared to ligand free flat porphyrin that is in full agreement with the previous theoretical<sup>[41,44,86,96,155]</sup> and experimental<sup>[41,44,79,96,152,156]</sup> works. Thus, Kolling et al.<sup>[91]</sup> and Nappa et al.<sup>[153]</sup> reported the experimentally obtained red shift of absorption B-band of up to 26.7 nm upon ligation of Zn complex of tetraphenylporphyrin. Also, Zhang et al.<sup>[86]</sup> measured the red shift of up to 17.8 nm for ligated saddled zinc porphyrin complexes.

Moreover, the energy gap between the third and fourth transitions is changed compared to that of flat porphyrins as with and without an axial ligand (Tables 4 and S9). The sole exception is ZnDP-NMe<sub>2</sub>, in which this shift is +2 and -2 nm for the third and fourth transition, correspondingly, that could be explained by inversion of these transitions. In fact, in flat ligated and non-ligated ZnDP-NMe<sub>2</sub> the third and the fourth transitions correspond to HOMO-2→LUMO and to HOMO-3→LUMO, respectively. However, in fully optimized ligated ZnDP-NMe<sub>2</sub> these transitions become the fifth and the sixth transitions, whilst HOMO-1→LUMO and HOMO-1→LUMO+1 become the third and the fourth transitions (Figure 12 and Table S9).

The absolute values of rotational strengths in fully optimized ligated porphyrins are significantly larger than those in flat ligand free porphyrins (showing nearly zero rotatory strengths) due to increase of the transition magnetic dipole moments and deviation of the angles between the transition electric and magnetic dipole moments from 90° (Table S11). The corresponding g-factors of ligated fully optimized porphyrins are comparable with those calculated for flat ligated



porphyrins and by 1–2 orders of magnitude larger than the *g*-factors of non-ligated porphyrins also showing the asymmetry generation by binding of a chiral guest.

The ECD spectra of fully optimized axially ligated porphyrins simulated using the cc-pVTZ basis set are shown in Figures 15 and S9. The ECD spectra of fully optimized ligated ZnP, ZnDP–OMe, ZnDP–OC(O)H and ZnDP–F remained almost unchanged as compared to those of flat ligated porphyrins. However, in the case of ZnDP–Me and ZnDP–NO<sub>2</sub> full optimization of the structures caused a significant increase of the B-band intensities as compared to flat ligated porphyrins (Figure S9). In several cases the profiles of the ECD spectra are drastically changed. For example, the transition sign of ZnDPP is switched from positive to negative as a result of optimization. In the case of ZnDPP–CF<sub>3</sub>-*p* and ZnDPP–NMe<sub>2</sub>-*p* a positive-to-negative bisignate signal appeared instead of a strong negative band observed for the corresponding ligated flat porphyrins. Most of these changes could be explained by coupling with peripheral substituents. Thus, in ligated fully optimized ZnP, ZnDP–F, ZnDP–CN, ZnDP–CF<sub>3</sub>, and ZnDP–Me the corresponding substituents are not chromophores resulting in the absence of coupling, and consequently only one negative band is observed. Despite of the different porphyrin plane distortion (small in ZnDP–Me and large in ZnDP–CF<sub>3</sub>) the intensities of these negative bands are comparable to be –11.0 cgs and –16.2 cgs, respectively (Table S9). Therefore, one may conclude that distortion of the porphyrin plane does not play a main role

in the ECD spectra formation. However, distortion of the porphyrin plane decreases the energy gap between LUMO and lower-energy HOMO-X, hence resulting in increase of the intensities of higher-energy transitions that in turn might be observed in the B region (for example, ZnDP–CF<sub>3</sub>, ZnDP–CN and ZnDP–NMe<sub>2</sub>). In the case of ligated fully optimized ZnDP–OMe, ZnDP–OC(O)H, ZnDP–NMe<sub>2</sub>, and ZnDP–NO<sub>2</sub> the tilt of peripheral substituents increases the intensities of the corresponding bands. If these substituents are in a conrotatory relative orientation, the intensities increased marginally (ZnDP–OC(O)H and ZnDP–NMe<sub>2</sub>), whilst a disrotatory orientation results in a more noticeable enhancement (ZnDP–NO<sub>2</sub>). However, the most drastic changes were caused by Ph and its derivatives in the disrotatory orientation where the ECD profile is significantly changed. For example, in ligated fully optimized ZnDPP the band sign is switched from positive to negative and in ligated fully optimized ZnDPP–NMe<sub>2</sub>-*p* a positive-to-negative bisignate signal appeared instead of a strong negative band observed for the corresponding flat porphyrin complexes. When the orientation of Ph and its derivatives is conrotatory, their influence on ECD spectra is also significant by decreasing the intensity of B-bands to some extent. Previously, LeCours et al.<sup>[62]</sup> based on the theoretical and experimental studies concluded that influence of the axial ligation on ECD spectra is smaller than that of porphyrin *meso*-substitution, however in this work it was clearly seen that both these effects act synergistically. Our results are in agreement with the experimental and theoretical works of Mizutani et al.<sup>[134,135]</sup> reported only one ECD signal for ligated zinc porphyrin complexes without peripheral chromophoric substituents and two bisignated ECD bands for ligated zinc porphyrin complexes with peripheral chromophoric substituents, which were fixed in a certain position by hydrogen bonds. The bisignated ECD bands were also measured in the works of Konrad et al.,<sup>[98]</sup> Imai et al.<sup>[157]</sup> and Balaz et al.<sup>[151]</sup> for ligated zinc porphyrin complexes with peripheral chromophoric substituents.

As mentioned above, when simulations were done using the aug-cc-pVDZ basis set, some differences in simulated ECD spectra were observed (Figure S9). In particular, ligated ZnDPP and ZnDPP–OMe-*p* exhibited negative bands with intensities of –11,3 and –11,4 cgs, respectively, which were larger than those obtained using the cc-pVTZ basis set (–4,2 and –2,0 cgs, respectively). In the cases of ligated ZnDPP–Me-*p* and ZnDPP–CF<sub>3</sub>-*p* only one positive band with intensities of +2,4 and +1,4 cgs, respectively was observed using the aug-cc-pVDZ basis set. In contrast, upon using the cc-pVTZ basis set a bisignate signal (with intensities of –0,2 and +0,3 cgs) and one negative signal (with intensities of –0,6 cgs) were observed for ZnDPP–Me-*p* and ZnDPP–CF<sub>3</sub>-*p*, respectively. However, the ECD spectra of all other ligated porphyrins were very similar regardless of the basis set used. Based on the data described above, the ECD spectra simulated using cc-pVTZ and aug-cc-pVDZ have a similar profile, while the intensities are varied. However, when the intensities are small (below 2,5 cgs) some differences in the shape and sign of ECD spectra upon using the cc-pVTZ and aug-cc-pVDZ basis sets are observed.

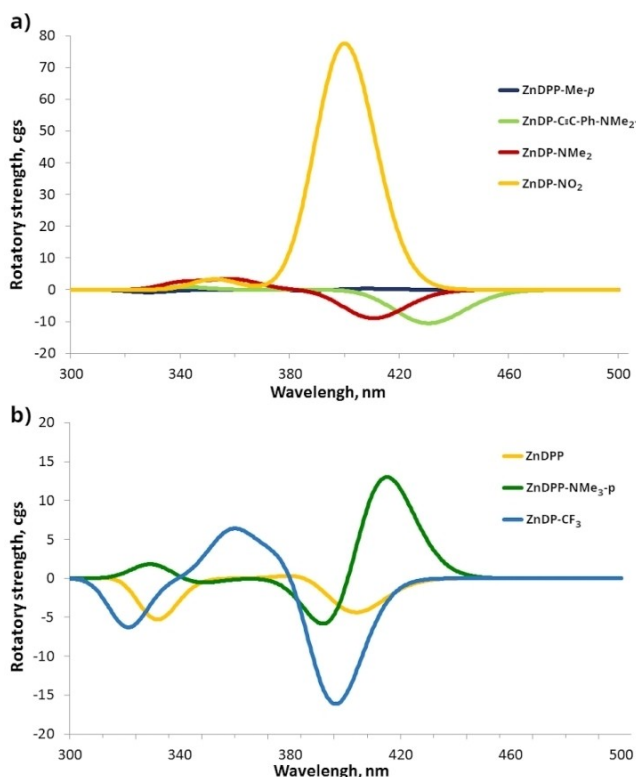


**Figure 15.** Simulated ECD spectra of ligated fully optimized a) ZnDPP–Me-*p*, ZnDP–C≡C–Ph–NMe<sub>2</sub>-*p*, ZnDP–NMe<sub>2</sub>, ZnDP–NO<sub>2</sub> and b) ZnDPP, ZnDP–NMe<sub>2</sub>-*p* and ZnDP–CF<sub>3</sub> calculated using ωB97X-D/cc-pVTZ.

In summary, it was found that axial ligation of porphyrins shifts the excitation energy to the lower-energy region and increases the energy gap between the two B electronic transitions. Moreover, the ECD spectra of axially ligated flat and fully optimized porphyrins are drastically different as a result of different orientations of the peripheral chromophoric substituents in fully optimized porphyrin complexes.

### 3. Conclusion

In this work, the six first electronic transitions of sixteen zinc porphyrins with and without an axial chiral ligand were calculated using the TD-DFT method,  $\omega$ B97X-D functional and two basis sets (cc-pVTZ and aug-cc-pVDZ). For non-silent ECD systems the corresponding spectra were simulated.

It can be concluded that all controlling factors, such as substituent's electron-donating/withdrawing effect, orientation of the peripheral substituents, deformation of the porphyrin plane, and axial ligation, affect the B electronic transitions and ECD spectra. The influence can be divided into two major contributions: excitation energy and rotational strength. The former is affected in the following order: orientation of the peripheral chromophoric substituents > substituent's effect > axial ligation. However, symmetrical deformation of the porphyrin plane has a negligible impact on the excitation energies. In the case of rotational strength, the influence increases as follows: substituent's effect < conrotatory orientation of the peripheral substituents < symmetrical deformation of the porphyrin plane < disrotatory orientation of the peripheral substituents < axial ligation. Also, it was found that coupling between the porphyrin and peripheral chromophoric substituents decreases the absolute values of rotational strengths.

This comprehensive theoretical analysis of various structural and supramolecular factors should have important implications for a judicious design of prospective efficient chirogenic systems on the basis of porphyrin chromophores.

### Computational Section

In this work the geometry optimization was performed using RI<sup>[158–160]</sup>-BP86<sup>[161,162]</sup>-D3<sup>[163]</sup>/def2-SV(P)<sup>[164]</sup> implemented in Turbomole 7.0<sup>[165]</sup> – the method which showed a good agreement with the experimental data reported in previous works.<sup>[98,99,166,167]</sup> The geometries of the complexes are given in SI.

The ECD spectra were simulated using the Gaussian16 Rev. B.01<sup>[168]</sup> software and TD-DFT method.<sup>[169–171]</sup> The simulations were done using the  $\omega$ B97X-D<sup>[172]</sup> functional, which previously showed a good agreement with the experimental spectra of zinc porphyrins,<sup>[98,99,166]</sup> and using the cc-pVTZ<sup>[173–177]</sup> and aug-cc-pVDZ<sup>[173,174,178]</sup> basis sets. The cc-pVTZ basis set was chosen, since its quality was enough for adequate description of the corresponding electric dipole moments and therefore rotatory strengths.<sup>[99,179–181]</sup> In addition to this basis set, a smaller basis set with diffused functions – aug-cc-pVDZ was tried, since in some works it was stated that the diffused functions are essential for ECD spectral simulations.<sup>[180–183]</sup> Also, previous investigation showed that a good correlation between the simulated and experimental spectra can be obtained already with the

DZVP basis set.<sup>[99,137,184]</sup> However, Nguyen et al.<sup>[185]</sup> and Theisen et al.<sup>[76]</sup> reported that particularly for porphyrin zinc complexes the polarization and diffuse functions have only a minor effect on the TD-DFT excitation energies of tetrapyrrolic compounds. In the present work both these functionals were used and the obtained results were compared. All simulations were performed using the SMD<sup>[186]</sup> continuum solvent model as it gives a better agreement with the experiment<sup>[99,166]</sup> and dichloromethane was chosen as one of the most popular solvents for ECD spectroscopy of porphyrins. The first six excited states were calculated in order to ensure that both the Q- and B-band regions of absorption spectrum are covered.

The ECD spectra were visualized using GaussView 6.1.<sup>[187]</sup> A bandwidth of 0.1 eV was used for spectral building and the rotatory strengths were calculated on the basis of the dipole velocity formalism, since it is origin independent.<sup>[181]</sup>

### Acknowledgements

This work was supported by the Estonian Research Council grant PUTJD749 (for I.O.) PRG399, (for R.A., V.B.) and the European Union's H2020-FETOPEN grant 828779 (INITIO) (for R.A., V.B.). Computations were performed on the Taltech High Performance Computing Centre (HPC Centre) and partly at the Computational Chemistry laboratory at Tallinn University of Technology, Estonia. I.O. acknowledges T. Tamm for his kind help.

### Conflict of Interest

The authors declare no conflict of interest.

**Keywords:** circular dichroism · density functional calculations · porphyrins · supramolecular chemistry · transition metals

- [1] C. M. Drain, A. Varotto, I. Radivojevic, *Chem. Rev.* **2009**, *109*, 1630–1658.
- [2] D. Voet, J. G. Voet, in *Biochemistry*, Wiley, **2004**, pp. 797–842.
- [3] M. O. Senge, S. A. MacGowan, J. M. O'Brien, *Chem. Commun.* **2015**, *51*, 17031–17063.
- [4] C.-M. Che, V. K.-Y. Lo, C.-Y. Zhou, J.-S. Huang, *Chem. Soc. Rev.* **2011**, *40*, 1950–1975.
- [5] J. C. Barona-Castaño, C. C. Carmona-Vargas, T. J. Brocksom, K. T. De Oliveira, *Molecules* **2016**, *21*, 310.
- [6] B. Meunier, *Chem. Rev.* **1992**, *92*, 1411–1456.
- [7] M. I. J. Stich, L. H. Fischer, O. S. Wolfbeis, *Chem. Soc. Rev.* **2010**, *39*, 3102–3114.
- [8] C. M. B. Carvalho, T. J. Brocksom, K. T. de Oliveira, *Chem. Soc. Rev.* **2013**, *42*, 3302–3317.
- [9] N. Chaudhri, M. Sankar, *RSC Adv.* **2015**, *5*, 3269–3275.
- [10] G. A. Hembury, V. V. Borovkov, Y. Inoue, *Chem. Rev.* **2008**, *108*, 1–73.
- [11] R. Paolesse, S. Nardis, D. Monti, M. Stefanelli, C. Di Natale, *Chem. Rev.* **2017**, *117*, 2517–2583.
- [12] Y. Ding, W.-H. Zhu, Y. Xie, *Chem. Rev.* **2017**, *117*, 2203–2256.
- [13] H. Lu, N. Kobayashi, *Chem. Rev.* **2016**, *116*, 6184–6261.
- [14] H. Lee, K.-I. Hong, W.-D. Jang, *Coord. Chem. Rev.* **2018**, *354*, 46–73.
- [15] P. C. A. Swamy, S. Mukherjee, P. Thilagar, *Anal. Chem.* **2014**, *86*, 3616–3624.
- [16] M. G. Walter, A. B. Rudine, C. C. Wamser, *J. Porphyrins Phthalocyanines* **2010**, *14*, 759–792.
- [17] M. V. Martínez-Díaz, G. de la Torre, T. Torres, *Chem. Commun.* **2010**, *46*, 7090–7108.

- [18] G. Bottari, O. Trukhina, M. Ince, T. Torres, *Coord. Chem. Rev.* **2012**, *256*, 2453–2477.
- [19] A. Günsel, E. Güzel, A. T. Bilgiçli, İ. Şişman, M. N. Yarasir, *J. Photochem. Photobiol. A* **2017**, *348*, 57–67.
- [20] X. Xue, A. Lindstrom, Y. Li, *Bioconjugate Chem.* **2019**, *30*, 1585–1603.
- [21] F. Cieplik, D. Deng, W. Crielard, W. Buchalla, E. Hellwig, A. Al-Ahmad, T. Maisch, *Crit. Rev. Microbiol.* **2018**, *44*, 571–589.
- [22] N. Tsolekile, S. Nelana, O. S. Oluwafemi, *Molecules* **2019**, *24*, 2669.
- [23] V. Borovkov, *Symmetry* **2010**, *2*, 184–200.
- [24] V. Borovkov, *Symmetry* **2014**, *6*, 256–294.
- [25] V. Borovkov, Y. Inoue, *Eur. J. Org. Chem.* **2009**, 189–197.
- [26] P. J. Chmielewski, M. Siczek, M. Stepień, *Chem. A Eur. J.* **2015**, *21*, 2547–2559.
- [27] M. Gaeta, R. Randazzo, D. A. Cristaldi, A. D'Urso, R. Purrello, M. E. Fragalà, *J. Porphyrins Phthalocyanines* **2017**, *21*, 426–430.
- [28] P. T. Mathew, F. Fang, *Engineering* **2018**, *4*, 760–771.
- [29] L. Cook, G. Brewer, W. Wong-Ng, *Crystals* **2017**, *7*, 223.
- [30] A. Y. Lebedev, M. A. Filatov, A. V. Cheprakov, S. A. Vinogradov, *J. Phys. Chem. A* **2008**, *112*, 7723–7733.
- [31] B. Ghanbari, L. Shahhoseini, M. Kubicki, *Polyhedron* **2017**, *133*, 419–432.
- [32] M. Ravikanth, T. K. Chandrashekar, in *Nonplanar porphyrins and their biological relevance: ground and excited state dynamics*, Springer, Berlin, Heidelberg, **1995**, pp. 105–188.
- [33] G. S. Ananthnag, V. S. Shetti, *Dalton Trans.* **2017**, *46*, 14062–14082.
- [34] T. Hoshi, N. Kobayashi, *Coord. Chem. Rev.* **2017**, *345*, 31–41.
- [35] M. Zawadzka, J. Wang, W. J. Blau, M. O. Senge, *Photochem. Photobiol. Sci.* **2013**, *12*, 996–1007.
- [36] S. N. Ghosh, in *Handbook of analytical techniques in concrete science and technology* (Ed.: V. S. Ramachandran, J. J. Beaudoin), William Andrew Publishing, Norwich, NY, **2001**, pp. 174–204.
- [37] J. Hu, Y. Xie, H. Zhang, C. He, Q. Zhang, G. Zou, *Chem. Commun.* **2019**, *55*, 4953–4956.
- [38] R. Wang, S. Chen, Q. Chen, H. Guo, F. Yang, *Dyes Pigment.* **2021**, *190*, 109332.
- [39] M. Urbanová, V. Setnicka, V. Král, K. Volka, *Biopolymers* **2001**, *60*, 307–316.
- [40] J. Ouyang, A. Swartjes, M. Geerts, P. J. Gilissen, D. Wang, P. C. P. Teeuwen, P. Tinnemans, N. Vanthuyne, S. Chentouf, F. P. J. T. Rutjes, J.-V. Naubron, J. Crassous, J. A. A. W. Elemans, R. J. M. Nolte, *Nat. Commun.* **2020**, *11*, 4776.
- [41] N. Chaudhri, R. J. Butcher, M. Sankar, *New J. Chem.* **2018**, *42*, 8190–8199.
- [42] M. Sharma, A. L. Ticho, L. Samankumara, M. Zeller, C. Brückner, *Inorg. Chem.* **2017**, *56*, 11490–11502.
- [43] E. A. Alemán, J. Joseph, D. A. Modarelli, *J. Org. Chem.* **2015**, *80*, 11031–11038.
- [44] J. Oh, H. Yoon, Y. M. Sung, P. Kang, M.-G. Choi, W.-D. Jang, D. Kim, *J. Phys. Chem. B* **2015**, *119*, 7053–7061.
- [45] J. Mack, M. J. Stillman, N. Kobayashi, *Coord. Chem. Rev.* **2007**, *251*, 429–453.
- [46] J. Mack, N. Kobayashi, *Chem. Rev.* **2011**, *111*, 281–321.
- [47] J. A. Shelnutz, X.-Z. Song, J.-G. Ma, S.-L. Jia, W. Jentzen, C. J. Medforth, C. J. Medforth, *Chem. Soc. Rev.* **1998**, *27*, 31–42.
- [48] K. M. Barkigia, L. Chantranupong, K. M. Smith, J. Fajer, *J. Am. Chem. Soc.* **1988**, *110*, 7566–7567.
- [49] K. M. Barkigia, M. W. Renner, L. R. Furenliid, C. J. Medforth, K. M. Smith, J. Fajer, *J. Am. Chem. Soc.* **1993**, *115*, 3627–3635.
- [50] C. J. Medforth, M. O. Senge, K. M. Smith, L. D. Sparks, J. A. Shelnutz, *J. Am. Chem. Soc.* **1992**, *114*, 9859–9869.
- [51] O. Cramariuc, T. I. Hukka, T. T. Rantala, *J. Phys. Chem. A* **2004**, *108*, 9435–9441.
- [52] Y. Song, R. E. Haddad, S.-L. Jia, S. Hok, M. M. Olmstead, D. J. Nurco, N. E. Schore, J. Zhang, J.-G. Ma, K. M. Smith, S. Gazeau, J. Pécaut, J.-C. Marchon, C. J. Medforth, J. A. Shelnutz, *J. Am. Chem. Soc.* **2005**, *127*, 1179–1192.
- [53] A. K. Wertsching, A. S. Koch, S. G. DiMaggio, *J. Am. Chem. Soc.* **2001**, *123*, 3932–3939.
- [54] H. Ryeng, A. Ghosh, *J. Am. Chem. Soc.* **2002**, *124*, 8099–8103.
- [55] R. E. Haddad, S. Gazeau, J. Pécaut, J.-C. Marchon, C. J. Medforth, J. A. Shelnutz, *J. Am. Chem. Soc.* **2003**, *125*, 1253–1268.
- [56] Z. Zhou, M. Shen, C. Cao, Q. Liu, Z. Yan, *Chem. A Eur. J.* **2012**, *18*, 7675–7679.
- [57] Z. Zhou, X. Zhou, Q. Liu, X. Zhang, H. Liu, *Org. Lett.* **2015**, *17*, 4078–4081.
- [58] M. J. Guberman-Pfeffer, J. A. Greco, L. P. Samankumara, M. Zeller, R. R. Birge, J. A. Gascón, C. Brückner, *J. Am. Chem. Soc.* **2017**, *139*, 548–560.
- [59] I. K. Thomassen, H. Vazquez-Lima, K. J. Gagnon, A. Ghosh, *Inorg. Chem.* **2015**, *54*, 11493–11497.
- [60] A. B. Graves, M. T. Graves, M. D. Liptak, *J. Phys. Chem. B* **2016**, *120*, 3844–3853.
- [61] C.-W. Lee, H.-P. Lu, C.-M. Lan, Y.-L. Huang, Y.-R. Liang, W.-N. Yen, Y.-C. Liu, Y.-S. Lin, E. W.-G. Diau, C.-Y. Yeh, *Chem. A Eur. J.* **2009**, *15*, 1403–1412.
- [62] S. M. LeCours, S. G. DiMaggio, M. J. Therien, *J. Am. Chem. Soc.* **1996**, *118*, 11854–11864.
- [63] S. J. Lind, K. C. Gordon, S. Gambhir, D. L. Officer, *Phys. Chem. Chem. Phys.* **2009**, *11*, 5598–5607.
- [64] P. J. Spellane, M. Gouterman, A. Antipas, S. Kim, Y. C. Liu, *Inorg. Chem.* **1980**, *19*, 386–391.
- [65] Y. Yamaguchi, *J. Chem. Phys.* **2005**, *122*, 184702.
- [66] P. J. Walsh, K. C. Gordon, D. L. Officer, W. M. Campbell, *J. Mol. Struct.* **2006**, *759*, 17–24.
- [67] Y. Saegusa, T. Ishizuka, T. Kojima, *Inorg. Chem.* **2018**, *57*, 1106–1115.
- [68] H.-H. (G.) Tsai, M. C. Simpson, *Chem. Phys. Lett.* **2002**, *353*, 111–118.
- [69] V. A. Walters, J. C. de Paula, B. Jackson, C. Nutaitis, K. Hall, J. Lind, K. Cardozo, G. Chandran, D. Raible, C. M. Phillips, *J. Phys. Chem.* **1995**, *99*, 1166–1171.
- [70] S. Hayashi, M. Tanaka, H. Hayashi, S. Eu, T. Umeyama, Y. Matano, Y. Araki, H. Imahori, *J. Phys. Chem. C* **2008**, *112*, 15576–15585.
- [71] N. A. Sánchez-Bojorge, G. Zaragoza-Galán, N. R. Flores-Holguín, M. A. Chávez-Rojo, C. Castro-García, L. M. Rodríguez-Valdez, *J. Mol. Struct.* **2019**, *1191*, 259–270.
- [72] E. Göransson, J. Boixel, C. Monnerau, E. Blart, Y. Pellegrin, H.-C. Becker, L. Hammarström, F. Odobel, *Inorg. Chem.* **2010**, *49*, 9823–9832.
- [73] R. Ma, P. Guo, H. Cui, X. Zhang, M. K. Nazeeruddin, M. Grätzel, *J. Phys. Chem. A* **2009**, *113*, 10119–10124.
- [74] J. Barbee, A. E. Kuznetsov, *Comput. Theor. Chem.* **2012**, *981*, 73–85.
- [75] F. Hajizadeh, A. Reisi-Vanani, Y. T. Azar, *Curr. Appl. Phys.* **2018**, *18*, 1122–1133.
- [76] R. F. Theisen, L. Huang, T. Fleetham, J. B. Adams, J. Li, *J. Chem. Phys.* **2015**, *142*, 94310.
- [77] L. Wu, F. Li, Y. Rao, B. Wen, L. Xu, M. Zhou, T. Tanaka, A. Osuka, J. Song, *Angew. Chem. Int. Ed.* **2019**, *58*, 8124–8128.
- [78] A. Muranaka, S. Homma, H. Maeda, H. Furuta, N. Kobayashi, *Chem. Phys. Lett.* **2008**, *460*, 495–498.
- [79] H. Wang, X. Wei, J. Li, *J. Porphyrins Phthalocyanines* **2018**, *22*, 953–964.
- [80] D. Sahoo, T. Guchhait, S. P. Rath, *Eur. J. Inorg. Chem.* **2016**, *2016*, 3441–3453.
- [81] Q. Liu, X. Zhang, W. Zeng, J. Wang, Z. Zhou, *J. Phys. Chem. B* **2015**, *119*, 14102–14110.
- [82] T. Sakai, Y. Ohgo, T. Ikeue, M. Takahashi, M. Takeda, M. Nakamura, *J. Am. Chem. Soc.* **2003**, *125*, 13028–13029.
- [83] R.-J. Cheng, Y.-K. Wang, P.-Y. Chen, Y.-P. Han, C.-C. Chang, *Chem. Commun.* **2005**, 1312–1314.
- [84] C. L. Lockhart, M. A. Conger, D. S. Pittman, M. D. Liptak, *J. Biol. Inorg. Chem.* **2015**, *20*, 757–770.
- [85] X.-T. Feng, J.-G. Yu, M. Lei, W.-H. Fang, S. Liu, *J. Phys. Chem. B* **2009**, *113*, 13381–13389.
- [86] J. Zhang, M. Tang, D. Chen, B. Lin, Z. Zhou, Q. Liu, *Inorg. Chem.* **2019**, *58*, 2627–2636.
- [87] M. A. Conger, A. R. Cornetta, M. D. Liptak, *Inorg. Chem.* **2019**, *58*, 15455–15465.
- [88] T. Kojima, T. Nakanishi, T. Honda, R. Harada, M. Shiro, S. Fukuzumi, *Eur. J. Inorg. Chem.* **2009**, *2009*, 727–734.
- [89] J. A. Shelnutz, *J. Am. Chem. Soc.* **1987**, *109*, 4169–4173.
- [90] S.-L. Jia, W. Jentzen, M. Shang, X.-Z. Song, J.-G. Ma, W. R. Scheidt, J. A. Shelnutz, *Inorg. Chem.* **1998**, *37*, 4402–4412.
- [91] O. W. Kolling, *Inorg. Chem.* **1979**, *18*, 1175–1176.
- [92] J. C. W. Chien, *J. Am. Chem. Soc.* **1978**, *100*, 1310–1312.
- [93] M. Y. R. Wang, B. M. Hoffman, *J. Am. Chem. Soc.* **1984**, *106*, 4235–4240.
- [94] G. Blauer, N. Sreerama, R. W. Woody, *Biochemistry* **1993**, *32*, 6674–6679.
- [95] N. Kobayashi, R. Higashi, B. C. Titeca, F. Lamote, A. Ceulemans, *J. Am. Chem. Soc.* **1999**, *121*, 12018–12028.
- [96] M. Nagai, C. Kobayashi, Y. Nagai, K. Imai, N. Mizusawa, H. Sakurai, S. Neya, M. Kayanuma, M. Shoji, S. Nagatomo, *J. Phys. Chem. B* **2015**, *119*, 1275–1287.
- [97] N. Angelini, N. Micali, P. Mineo, E. Scamporrino, V. Villari, D. Vitalini, *J. Phys. Chem. B* **2005**, *109*, 18645–18651.



- [98] N. Konrad, D. Menialava, I. Osadchuk, J. Adamson, M. Hasan, E. Clot, R. Aav, V. Borovkov, D. Kananovich, *J. Porphyrins Phthalocyanines* **2019**, *24*, 840–849.
- [99] I. Osadchuk, V. Borovkov, R. Aav, E. Clot, *Phys. Chem. Chem. Phys.* **2020**, *22*, 11025–11037.
- [100] M. Ravikanth, D. Reddy, T. K. Chandrashekar, *Chem. Phys. Lett.* **1994**, *222*, 563–570.
- [101] C. Ngaojampa, S. Namuangruk, Y. Surakhot, V. Promarak, S. Jungsuttiwong, N. Kungwan, *Comput. Theor. Chem.* **2015**, *1062*, 1–10.
- [102] P. J. Walsh, K. C. Gordon, P. Wagner, D. L. Officer, *ChemPhysChem* **2006**, *7*, 2358–2365.
- [103] H. van der Salm, P. Wagner, K. Wagner, D. L. Officer, G. G. Wallace, K. C. Gordon, *Chem. A Eur. J.* **2015**, *21*, 15622–15632.
- [104] P. Bhyrappa, M. Sankar, B. Varghese, *Inorg. Chem.* **2006**, *45*, 4136–4149.
- [105] J. C. Earles, K. C. Gordon, A. W. I. Stephenson, A. C. Partridge, D. L. Officer, *Phys. Chem. Chem. Phys.* **2011**, *13*, 1597–1605.
- [106] P. Bhyrappa, *Tetrahedron Lett.* **2016**, *57*, 5150–5167.
- [107] J. Rochford, D. Chu, A. Hagfeldt, E. Galoppini, *J. Am. Chem. Soc.* **2007**, *129*, 4655–4665.
- [108] V. P. Nicu, A. Mándi, T. Kurtán, P. L. Polavarapu, *Chirality* **2014**, *26*, 525–531.
- [109] M. Ptaszek, in *Fluoresc. Biosens.* (Ed.: M. C. Morris), Academic Press, **2013**, pp. 59–108.
- [110] J. Mack, *Chem. Rev.* **2017**, *117*, 3444–3478.
- [111] M. P. Balanay, D. H. Kim, *Phys. Chem. Chem. Phys.* **2008**, *10*, 5121–5127.
- [112] C. Farley, N. V. S. D. K. Bhupathiraju, B. K. John, C. M. Drain, *J. Phys. Chem. A* **2016**, *120*, 7451–7464.
- [113] S. Neya, M. Nagai, S. Nagatomo, T. Hoshino, T. Yoneda, A. T. Kawaguchi, *Biochim. Biophys. Acta Bioenerg.* **2016**, *1857*, 582–588.
- [114] N. Grover, M. Sankar, Y. Song, K. M. Kadish, *Inorg. Chem.* **2016**, *55*, 584–597.
- [115] P. Bhyrappa, B. Purushothaman, *J. Chem. Soc. Perkin Trans. 2* **2001**, 238–242.
- [116] B. Hu, M. He, Z. Yao, C. E. Schulz, J. Li, *Inorg. Chem.* **2016**, *55*, 9632–9643.
- [117] C. Kiefl, N. Sreerama, R. Haddad, L. Sun, W. Jentzen, Y. Lu, Y. Qiu, J. Shelnutt, R. Woody, *J. Am. Chem. Soc.* **2002**, *124*, 3385–3394.
- [118] M. Gouterman, *J. Mol. Spectrosc.* **1961**, *6*, 138–163.
- [119] M. Gouterman, G. H. Wagnière, L. C. Snyder, *J. Mol. Spectrosc.* **1963**, *11*, 108–127.
- [120] N. Kobayashi, H. Ogata, N. Nonaka, E. A. Luk'yanets, *Chem. A Eur. J.* **2003**, *9*, 5123–5134.
- [121] Y. Rio, M. Salomé Rodríguez-Morgade, T. Torres, *Org. Biomol. Chem.* **2008**, *6*, 1877–1894.
- [122] R. Li, X. Zhang, P. Zhu, D. K. P. Ng, N. Kobayashi, J. Jiang, *Inorg. Chem.* **2006**, *45*, 2327–2334.
- [123] H. Shinohara, O. Tsaryova, G. Schnurpfeil, D. Wöhrle, *J. Photochem. Photobiol. A* **2006**, *184*, 50–57.
- [124] M.-S. Liao, S. Scheiner, *Chem. Phys. Lett.* **2003**, *367*, 199–206.
- [125] S. A. Sibilia, R. S. Czernuszewicz, M. J. Crossley, T. G. Spiro, *Inorg. Chem.* **1997**, *36*, 6450–6453.
- [126] R. A. Binstead, M. J. Crossley, N. S. Hush, *Inorg. Chem.* **1991**, *30*, 1259–1264.
- [127] M. Zawadzka, J. Wang, W. J. Blau, M. O. Senge, *Chem. Phys. Lett.* **2009**, *477*, 330–335.
- [128] A. Nowak-Król, C. J. Wilson, M. Drobizhev, D. V. Kondratuk, A. Rebane, H. L. Anderson, D. T. Gryko, *ChemPhysChem* **2012**, *13*, 3966–3972.
- [129] C.-W. Huang, K. Yuan Chiu, S.-H. Cheng, *Dalton Trans.* **2005**, 2417–2422.
- [130] N. C. M. Magdaong, M. Taniguchi, J. R. Diers, D. M. Niedzwiedzki, C. Kirmaier, J. S. Lindsey, D. F. Bocian, D. Holten, *J. Phys. Chem. A* **2020**, *124*, 7776–7794.
- [131] L. Angiolini, T. Benelli, L. Giorgini, *React. Funct. Polym.* **2011**, *71*, 204–209.
- [132] V. V. Borovkov, J. M. Lintuluoto, Y. Inoue, *J. Am. Chem. Soc.* **2001**, *123*, 2979–2989.
- [133] J. Rochford, S. Botchway, J. J. McGarvey, A. D. Rooney, M. T. Pryce, *J. Phys. Chem. A* **2008**, *112*, 11611–11618.
- [134] T. Mizutani, T. Ema, T. Yoshida, Y. Kuroda, H. Ogoshi, *Inorg. Chem.* **1993**, *32*, 2072–2077.
- [135] T. Mizutani, T. Ema, T. Yoshida, T. Renne, H. Ogoshi, *Inorg. Chem.* **1994**, *33*, 3558–3566.
- [136] X.-C. Li, D. Ferreira, Y. Ding, *Curr. Org. Chem.* **2010**, *14*, 1678–1697.
- [137] Y. Si, G. Yang, *RSC Adv.* **2013**, *3*, 2241–2247.
- [138] H.-H. G. Tsai, M. C. Simpson, *J. Phys. Chem. A* **2004**, *108*, 1224–1232.
- [139] W. Jentzen, X. Z. Song, J. A. Shelnutt, *J. Phys. Chem. B* **1997**, *101*, 1684–1699.
- [140] W. Jentzen, E. Unger, X.-Z. Song, S.-L. Jia, I. Turowska-Tyrk, R. Schweitzer-Stenner, W. Dreybrodt, W. R. Scheidt, J. A. Shelnutt, *J. Phys. Chem. A* **1997**, *101*, 5789–5798.
- [141] W. Jentzen, J.-G. Ma, J. A. Shelnutt, *Biophys. J.* **1998**, *74*, 753–763.
- [142] D. Gibbons, K. J. Flanagan, L. Pounot, M. O. Senge, *Photochem. Photobiol. Sci.* **2019**, *18*, 1479–1494.
- [143] M. P. Austeria, P. D. Pancharatna, M. M. Balakrishnarajan, *Eur. J. Inorg. Chem.* **2014**, *2014*, 3200–3207.
- [144] A. B. Graves, R. P. Morse, A. Chao, A. Iniguez, C. W. Goulding, M. D. Liptak, *Inorg. Chem.* **2014**, *53*, 5931–5940.
- [145] J. Kaminský, J. Kubelka, P. Bouř, *J. Phys. Chem. A* **2011**, *115*, 1734–1742.
- [146] J. L. Retsek, C. J. Medforth, D. J. Nurco, S. Gentemann, V. S. Chirvony, K. M. Smith, D. Holten, *J. Phys. Chem. B* **2001**, *105*, 6396–6411.
- [147] A. B. J. Parusel, T. Wondimagegn, A. Ghosh, *J. Am. Chem. Soc.* **2000**, *122*, 6371–6374.
- [148] J. K. Choi, A. D'Urso, M. Balaz, *J. Inorg. Biochem.* **2013**, *127*, 1–6.
- [149] A. C. Gehrold, T. Bruhn, H. Schneider, U. Radius, G. Bringmann, *J. Org. Chem.* **2015**, *80*, 12359–12378.
- [150] Z. Yao, C. E. Schulz, N. Zhan, J. Li, *Inorg. Chem.* **2017**, *56*, 12615–12624.
- [151] A. D'Urso, A. E. Holmes, N. Berova, M. Balaz, R. Purrello, *Chem. Asian J.* **2011**, *6*, 3104–3109.
- [152] C. Lin, M.-Y. Fang, S.-H. Cheng, *J. Electroanal. Chem.* **2002**, *531*, 155–162.
- [153] M. Nappa, J. S. Valentine, *J. Am. Chem. Soc.* **1978**, *100*, 5075–5080.
- [154] Scholarly Community Encyclopedia <https://encyclopedia.pub/212> (accessed July 11, 2021)..
- [155] K. Oberda, I. Deperasińska, Y. P. Nizhnik, A. Szemik-Hojniak, *Polyhedron* **2013**, *51*, 61–69.
- [156] K. Oberda, I. Deperasińska, Y. Nizhnik, L. Jerzykiewicz, A. Szemik-Hojniak, *Polyhedron* **2011**, *30*, 2391–2399.
- [157] H. Imai, H. Munakata, Y. Uemori, N. Sakura, *Inorg. Chem.* **2004**, *43*, 1211–1213.
- [158] K. Eichkorn, F. Weigend, O. Treutler, R. Ahlrichs, *Theor. Chem. Acc.* **1997**, *97*, 119–124.
- [159] K. Eichkorn, O. Treutler, H. Öhm, M. Häser, R. Ahlrichs, *Chem. Phys. Lett.* **1995**, *240*, 283–290.
- [160] M. Sierka, A. Hogekamp, R. Ahlrichs, *J. Chem. Phys.* **2003**, *118*, 9136–9148.
- [161] A. D. Becke, *Phys. Rev. A* **1988**, *38*, 3098–3100.
- [162] J. P. Perdew, *Phys. Rev. B* **1986**, *33*, 8822–8824.
- [163] S. Grimme, J. Antony, S. Ehrlich, H. Krieg, *J. Chem. Phys.* **2010**, *132*, 154104.
- [164] A. Schäfer, H. Horn, R. Ahlrichs, *J. Chem. Phys.* **1992**, *97*, 2571–2577.
- [165] TURBOMOLE V7.0 2015, a development of University of Karlsruhe and Forschungszentrum Karlsruhe GmbH, 1989–2007, TURBOMOLE GmbH, since 2007; available from <http://www.turbomole.com>.
- [166] A. G. Martynov, J. Mack, A. K. May, T. Nyokong, Y. G. Gorbunova, A. Y. Tsvadze, *ACS Omega* **2019**, *4*, 7265–7284.
- [167] N. Schmidt, R. Fink, W. Hieringer, *J. Chem. Phys.* **2010**, *133*, 54703.
- [168] M. J. Frisch, G. W. Trucks, H. B. Schlegel, G. E. Scuseria, M. A. Robb, J. R. Cheeseman, G. Scalmani, V. Barone, G. A. Petersson, H. Nakatsuji, X. Li, M. Caricato, A. V. Marenich, J. Bloino, B. G. Janesko, R. Gomperts, B. Mennucci, H. P. Hratchian, J. V. Ortiz, A. F. Izmaylov, J. L. Sonnenberg, D. Williams-Young, F. Ding, F. Lipparini, F. Egidi, J. Goings, B. Peng, A. Petrone, T. Henderson, D. Ranasinghe, V. G. Zakrzewski, J. Gao, N. Rega, G. Zheng, W. Liang, M. Hada, M. Ehara, K. Toyota, R. Fukuda, J. Hasegawa, M. Ishida, T. Nakajima, Y. Honda, O. Kitao, H. Nakai, T. Vreven, K. Throssell, J. A. Montgomery Jr, J. E. Peralta, F. Ogliaro, M. J. Bearpark, J. J. Heyd, E. N. Brothers, K. N. Kudin, V. N. Staroverov, T. A. Keith, R. Kobayashi, J. Normand, K. Raghavachari, A. P. Rendell, J. C. Burant, S. S. Iyengar, J. Tomasi, M. Cossi, J. M. Millam, M. Klene, C. Adamo, R. Cammi, J. W. Ochterski, R. L. Martin, K. Morokuma, O. Farkas, J. B. Foresman, D. J. Fox, Gaussian 16, Revision B.01, Gaussian, Inc., Wallingford CT, **2016**.
- [169] R. Bauernschmitt, R. Ahlrichs, *Chem. Phys. Lett.* **1996**, *256*, 454–464.
- [170] R. E. Stratmann, G. E. Scuseria, M. J. Frisch, *J. Chem. Phys.* **1998**, *109*, 8218–8224.
- [171] M. E. Casida, C. Jamorski, K. C. Casida, D. R. Salahub, *J. Chem. Phys.* **1998**, *108*, 4439–4449.
- [172] J.-D. Chai, M. Head-Gordon, *Phys. Chem. Chem. Phys.* **2008**, *10*, 6615–6620.
- [173] T. H. Dunning, *J. Chem. Phys.* **1989**, *90*, 1007–1023.
- [174] D. E. Woon, T. H. Dunning, *J. Chem. Phys.* **1993**, *98*, 1358–1371.



- [175] K. A. Peterson, D. E. Woon, T. H. Dunning, *J. Chem. Phys.* **1994**, *100*, 7410–7415.
- [176] A. C. Tsipis, *Coord. Chem. Rev.* **2014**, *272*, 1–29.
- [177] A. Jesser, M. Rohrmüller, W. G. Schmidt, S. Herres-Pawlis, *J. Comput. Chem.* **2014**, *35*, 1–17.
- [178] R. A. Kendall, T. H. Dunning, R. J. Harrison, *J. Chem. Phys.* **1992**, *96*, 6796–6806.
- [179] A. Rizzo, O. Vahtras, *J. Chem. Phys.* **2011**, *134*, 244109.
- [180] H. Jang, N. J. Kim, J. Heo, *Comput. Theor. Chem.* **2018**, *1125*, 63–68.
- [181] I. Warnke, F. Furche, *Wiley Interdiscip. Rev.: Comput. Mol. Sci.* **2012**, *2*, 150–166.
- [182] D. Jacquemin, C. Adamo, *Int. J. Quantum Chem.* **2012**, *112*, 2135–2141.
- [183] M. Pecul, K. Ruud, *Adv. Quantum Chem.* **2005**, *50*, 185–212.
- [184] K. Nakano, T. Konishi, Y. Imamura, *Chem. Phys.* **2019**, *518*, 15–24.
- [185] K. A. Nguyen, R. Pachter, *J. Chem. Phys.* **2001**, *114*, 10757–10767.
- [186] A. V. Marenich, C. J. Cramer, D. G. Truhlar, *J. Phys. Chem. B* **2009**, *113*, 6378–6396.
- [187] R. Dennington, T. A. Keith, J. M. Millam, Semichem Inc., GaussView, Version 6.1, Shawnee Mission, KS, **2016**.

---

Manuscript received: May 4, 2021

Revised manuscript received: June 24, 2021

Accepted manuscript online: July 2, 2021

Version of record online: July 12, 2021